Patch-Wise Random and Noisy CutMix for Privacy-Preserving Split Learning with Vision Transformer

Anonymous authors
Paper under double-blind review

Abstract

In computer vision, the vision transformer (ViT) has increasingly superseded the convolutional neural network (CNN) for improved accuracy and robustness. Since ViT often comes with large model sizes and high sample complexity, split learning (SL) is a promising solution to training ViT using large memory and computing resources at a server with the sheer amount of private data owned by users or clients. In SL, a ViT is split into two parts under a server-client architecture. The sever stores its upper segment that is associated with multiple clients each of which stores the lower segment. At the cut layer between the upper and lower segments, SL exchanges the cut-layer hidden activations in the forward propagation (FP), referred to as smashed data, and the cut-layer gradients in the backpropagation (BP), which are exposed to various attacks on private training data. To mitigate the risk of data breaches in classification tasks, inspired from the CutMix regularization, we propose a novel privacy-preserving SL framework that injects Gaussian noise into smashed data and mixes randomly chosen patches of smashed data across clients, coined *DP-CutMixSL*. By analysis, we prove that DP-CutMixSL is a differentially private (DP) mechanism amplifying the privacy budget with respect to membership inference attacks in FP. By simulation, we additionally show that DP-CutMixSL protects privacy from reconstruction attacks in FP and from label inference attacks in BP. Surprisingly, DP-CutMixSL even improves accuracy and robustness to imbalanced data distributions over clients, due to the regularization effect of its patch-wise random CutMix operations.

1 Introduction

Transformer architecture has originally been developed in the domain of natural language processing (NLP) Vaswani et al. (2017), and its application has recently been extended to various domains including speech recognition Karita et al. (2019) and computer vision (CV) Dosovitskiy et al. (2020b). In particular, the *vision transformer (ViT)* has recently been the new standard architecture in CV, succeeded to the convolutional neural network (CNN) architecture. ViT operations are summarized in two steps: 1) the first step to dividing image data into multiple image *patches*, and 2) the second step to learning the relationship between the patches under the encoder of the transformer. The latter step, dubbed the *self-attention* mechanism, helps to achieve high performance on large datasets, but causes performance degradation on small datasets due to its weak inductive bias. Hence, securing large-scale datasets in ViT is essential yet challenging, especially in distributed learning scenarios where huge data is dispersed to multiple *clients* with limited computing capability Khan et al. (2021); Han et al. (2022). Federated learning (FL) is a promising solution in terms of enjoying these scattered data and computing resources Li et al. (2020); Kairouz et al. (2021). In FL, each client trains a local model to be uploaded to the *server* with their own dataset, while the server yields the global model by taking the weighted average of the local models, leading to data diversity gain without direct data exchange. Such model averaging, however, makes FL not suitable for ViT, which is computationally expensive and often has a large model size.

To cope with this, *split learning (SL)* can be an alternative solution in a sense that the client and server divide the entire model into two fractions, a *lower model segment* and an *upper model segment*, and store each one Gupta and Raskar (2018); Vepakomma et al. (2018). Under this model-split architecture, clients

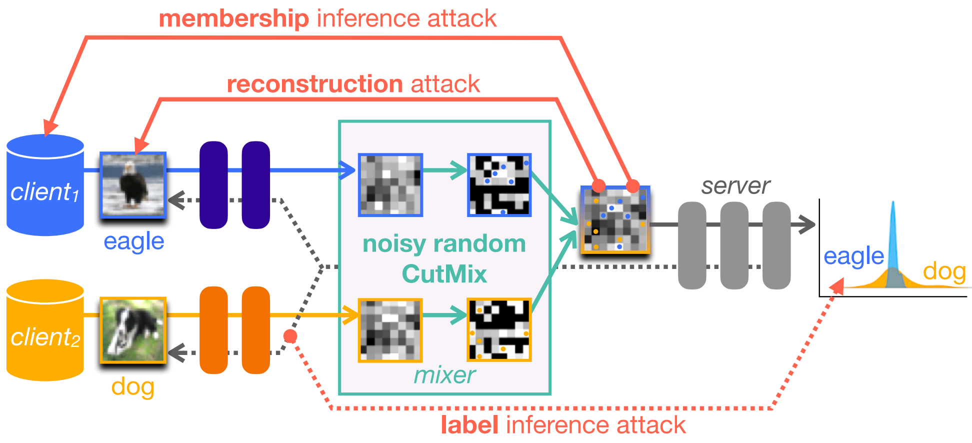

Figure 1: A schematic illustration of DP-CutMixSL with 2 clients.

upload a cut-layer representation, also referred to as *smashed data*, from the SL's forward propagation (FP) and download its corresponding gradient from the SL's backward propagation (BP). However, unlike CNN's smashed data, the smashed data of ViT is not actually "smashed" due to the absence of such a pooling layer, questioning SL's data privacy guarantee.

To this end, we propose a novel distributed learning framework for ViT, coined *DP-CutMixSL*, that is differentially private (DP) under the parallel SL (PSL) architecture. Influenced by CutMix regularization Yun et al. (2019), each client of DP-CutMixSL uploads its own masked smashed data, whose masks are mutually exclusive collectively exhaustive (MECE) in patch-wise, with additive Gaussian noise. Precisely, a novel entity, the *mixer*, generates the two MECE and binary masks with a dirichlet-multinomial distribution Bishop et al. (2007), which are distributed to each of the two clients. Here, the mixer aims to operate while maintaining data privacy to the server, and is implemented through homomorphic encryption Rivest et al. (1978); Pereteanu et al. (2022) or analog communication Koda et al. (2021). Then, each client injects noise following a Gaussian mechanism Abadi et al. (2016); Gil et al. (2013); Girgis et al. (2021) into the smashed data, and returns only a fraction of it, dubbed *DP-Cutout smashed data*, to the mixer according to the mask. Next, the mixer combines aggregated DP-Cutout smashed data to yield *DP-CutMix smashed data*, followed by the remaining operations of PSL including server-side FP-BP.

In doing so, DP-CutMixSL is beneficial in terms of robustness against various privacy attacks shown in figure 1. Regarding privacy attacks in SL, membership inference attack Shokri et al. (2017); Rahman et al. (2018) and model inversion attack or reconstruction attack He et al. (2019) in FP try to determine whether or not data is used and restore input data, respectively, while label inference attack Li et al. (2021); Yang et al. (2022) in BP infers the label through the gradient of the cut-layer. Thanks to its randomly punched smashed data as well as Gaussian noise, DP-CutMixSL can provide a strong privacy guarantee under these privacy attacks. Meanwhile, DP-CutMixSL shows improved performance in accuracy and communication-efficiency, thanks to its inherent regularization effect.

Contributions. The key contributions of this article are summarized as follows[1]:

- Inspired by CutMix, we propose a new SL-based architecture named DP-CutMixSL aiming to improve privacy guarantee and communication-efficiency of ViT. In this process, we introduce an entity called mixer on a network consisting of client-server, and define its operations such as pseudorandom sequence generation for yielding DP-Cutout smashed data and further DP-CutMix smashed data.

- We theoretically derive the privacy guarantee of DP-CutMixSL against membership inference attacks through DP analysis and experimentally demonstrate it.

[1] This work is an extended version of both our previous workshop papers Baek et al. (2022); Oh et al. (2022a), with the addition of extensive experiments involving label inference attacks and an analysis of the subsampled mechanism.

- Through experiments, we verify that DP-CutMixSL is robust against reconstruction attack and label inference attack.
- In addition, we show that DP-CutMixSL outperforms baselines such as PSL and split federated learning (SFL) in terms of accuracy and communication-efficiency via numerical evaluation.

2 Related Works

Vision Transformers. The transformer architecture is first used in the NLP field Vaswani et al. (2017), where its core operation is rooted on self-attention mechanism as well as encoder structure with multi-layer perceptron (MLP) and residual connection. In NLP, such transformer-based architecture is extended from Bidirectional Encoder Representations from Transformers (BERT) Devlin et al. (2018), Generative Pre-trained Transformer (GPT) Radford et al. (2018) to GPT-2 Radford et al. (2019), GPT-3 Brown et al. (2020). This paradigm shift from CNN to transformer has reached out to the CV field. ViT, proposed in Dosovitskiy et al. (2020a), is the first of its kind to apply the transformer architecture to the CV field. ViT transforms an input image into a series of image patches, just as a transformer embeds words in text, and learns relationships between image patches, thereby a large-scale dataset is indispensible. This ViT operation enables to extract global spatial information, leading to its robustness against information loss such as patch drop and image shuffling compared to CNN Naseer et al. (2021).

If most of the ViT works are based on the centralized method Carion et al. (2020); Zheng et al. (2021); Chen et al. (2021), several studies have conducted research on distributed implementation of transformer or ViT Hong et al. (2021); Park et al. (2021b); Qu et al. (2021). Hong et al. (2021) has designed FL-based transformer structure targeting text to speech task, while Qu et al. (2021) has explored the performance of FL in ViT when data are heterogeneous. To diagnose COVID-19, Park et al. (2021b) proposed SL-based architecture in ViT, benefiting from its robustness on task-agnostic training.

Federated & Split Learning. The key element of the distributed learning framework is to utilize raw data and computing resources spread across the sheer amount of Internet-of-Things (IoT) devices or clients. As the first kind of this, FL enables to acquire data diversity gain through exchanging model parameters Li et al. (2020); Kairouz et al. (2021). FL's model parameter aggregation does not induce data privacy leakage, and what is more, it ensures scalability in terms of increasing accuracy with the number of participating clients Konečnỳ et al. (2015); Park et al. (2021a). Nevertheless, FL has a trouble in running a large-size model, constrained by its limited client-side computation and communication resources, highlighting the need for alternative solutions Konečnỳ et al. (2016); Singh et al. (2019). To this end, SL has appeared as a enabler for large model operation by splitting the entire model into two partitions Gupta and Raskar (2018); Vepakomma et al. (2018); Gao et al. (2020). The initial implementation of SL, which is based on sequential method, used to result in large latency especially with many clients, giving rise to the research on PSL free from this problem. SFL, a combination of FL and SL, is the first form of PSL, allowing simultaneous access by multiple clients Thapa et al. (2020a;b); Gao et al. (2021). One step further, Pal et al. (2021) and Oh et al. (2022b) try to address the low accuracy, communication efficiency, and scalability of SFL.

Privacy Attacks & Differential Privacy. As machine learning develops rapidly, several types of privacy attacks have emerged whose goal is to extract information about training data, labels or the model itself. In particular, regarding the privacy attack on distributed learning, Nasr et al. (2018) shows the membership inference attack of an adversary with some auxiliary information on the training data. He et al. (2019) investigates the reconstruction attack occurring on the inference phase of vanilla SL under white-box and black-box settings, while Oh et al. (2022b) measures it emprically on the PSL structure. In addition, for label inference attacks in vanilla SL, Li et al. (2021) handles norm-based and direction-based attacks under black-box setting, and Yang et al. (2022) deals with white-box attacks and GradPerturb as a solution for them.

Accordingly, many studies have been conducted to protect information from various privacy attacks. One line of works first introduced the application of DP analysis technique to deep learning models Dwork (2008); Abadi et al. (2016). PixelDP, designed for SFL, is proposed as a DP-based defence to adversarial examples, providing certified robustness to AI/ML models, while Wu et al. (2022) applies the concept of DP to FL.

Meanwhile, Reńyi DP (RDP) is presented to facilitate the composition between heterogeneous mechanisms while providing tight bounds with fewer computations Mironov (2017). Such DP or RDP bounds can be tighter through Mixup Zhang et al. (2017); Verma et al. (2019) with the help of its inherent distortion property Koda et al. (2021); Borgnia et al. (2021); Lee et al. (2019). Another privacy amplification is possible via subsampling Balle et al. (2018) as well as shuffling Erlingsson et al. (2019).

3 DP-CutMixSL: Split Learning With Random CutMix for ViT

In this section, we demonstrate a proposed *differentially private CutMixSL (DP-CutMixSL)* framework, aiming to improve ViT's privacy guarantee while still ensuring its accuracy or communication-efficiency. Starting from the ViT operation based on the PSL structure, we describe Random Cutout to Random CutMix sequentially. Also, each subsection clarifies the key design elements of them in detail.

Consider a network with a set of clients $\mathbb{C} = \{1, 2, \cdots, n\}$ and a single server. Here, let i be the subscript for the client. The dataset of the i-th client is expressed as $\mathbb{D}_i$, consisting of multiple tuples of input data $\mathbf{x}_i$ and its one-hot encoded ground-truth label $\mathbf{y}_i$. We denote the i-th entire network as $\mathbf{w}_i = [\mathbf{w}_{c,i}, \mathbf{w}_s]^{\mathrm{T}}$, where $\mathbf{w}_{c,i}$, $\mathbf{w}_s$, and $(\cdot)^{\mathrm{T}}$ represent the i-th lower model segment, the upper model segment, and the transpose function, respectively. In addition, f_i and g indicate mapping from input data to smashed data via $\mathbf{w}_{c,i}$ and mapping from smashed data to output via $\mathbf{w}_s$, while P means patch size.

A Parallel Split Learning

This subsection first revisits the PSL operation on ViT. For the sake of convenience, we assume that the cut-layer is located between the embedding layer and the transformer in the ViT structure, so that the client converts the input image into *embedded patches* through the lower model segment, followed by the server forward and back propagates it through the upper model segment.

Patch Embedding. At the i-th client, the input data $\mathbf{x}_i \in \mathbb{R}^{H\times W\times C}$ is first divided into N image patches, so that $\mathbf{x}_i$ is transformed into $\mathbf{x}'_i \in \mathbb{R}^{N\times P^2\times C}$, where the number of image patches N equals to $\frac{H\cdot W}{P^2}$. Then, each image patch is linearly projected, whose dimension changes from $P^2 \times C$ to $1 \times (P^2 \times C)$. When the flattened patch size is denoted as $D_p = P^2 \times C$, a *class token* of the same size as D_p is attached in front of N image patches, resulting in $\mathbf{x}''_i$ where its dimension equals to $D_s = (N+1) \times D_p$. Finally, an embedding vector of its size D_s is added to $\mathbf{x}''_i$ for positional embedding, producing embedded patches $\mathbf{s}_i = [\mathbf{s}_{i,0}, \mathbf{s}_{i,1}, \cdots, \mathbf{s}_{i,N}]$ corresponding to the smashed data on ViT with PSL. This completes the 1D embedding step that generates the transformer's input. Note that the positional embedding is trainable and parameterizable with $\mathbf{w}_{c,i}$. We abbreviate the smashed data obtained through the entire 1D embedding process above as follows:

$$\mathbf{s}_i = f_i(\mathbf{x}_i). \tag{1}$$

FP & BP in Transformer. At the server, $\mathbf{s}_i$ for all $i \in \mathbb{C}$ is aggregated and passes through the upper model segment $\mathbf{w}_s$ to yield *softmax output* denoted by $g(\mathbf{s}_i)$. Using the cross entropy function $CE(p, q) = -\sum_j q_j \log p_j$ where j is the subscript for the element, the loss for the i-th smashed data can be represented as $L_i = CE(g(\mathbf{s}_i), \mathbf{y}_i)$. If we generalize this to batch $\mathbb{B}_i \subset \mathbb{D}_i$ of size b, L_i becomes:

$$L_i = \frac{1}{b} \sum_{(\mathbf{x}_i, \mathbf{y}_i)\in\mathbb{B}_i} CE(g(f_i(\mathbf{x}_i)), \mathbf{y}_i). \tag{2}$$

For all i, based on loss L_i, the server sends the i-th cut-layer gradient indicated by $\nabla_{\mathbf{s}_i} L_i$ to the i-th client, enabling weight update in the server and client as in the following formula:

$$\begin{bmatrix} \mathbf{w}_s \\ \mathbf{w}_{c,i} \end{bmatrix} \leftarrow \begin{bmatrix} \mathbf{w}_s \\ \mathbf{w}_{c,i} \end{bmatrix} - \eta \begin{bmatrix} \sum_{i\in\mathbb{C}} d_i \cdot (\nabla_{\mathbf{w}_s} L_i) \\ \nabla_{\mathbf{w}_{c,i}} L_i \end{bmatrix}, \tag{3}$$

where η is the learning rate and $d_i = |\mathbb{D}_i| / \sum_i |\mathbb{D}_i|$.

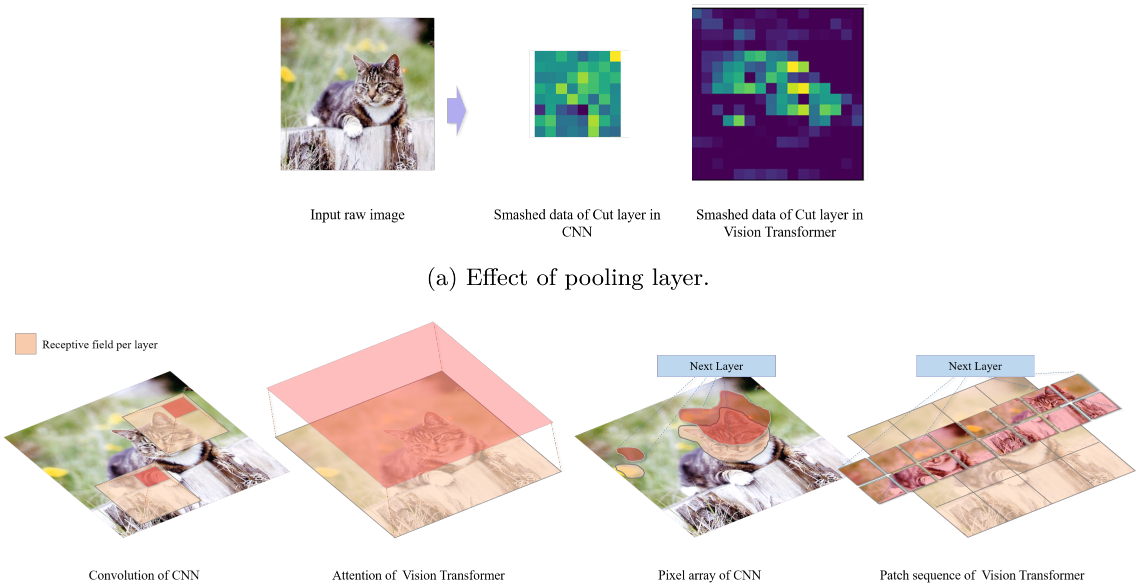
Input raw image
Smashed data of Cut layer in CNN
Smashed data of Cut layer in Vision Transformer
Receptive field per layer
Next Layer
Next Layer
Convolution of CNN
Attention of Vision Transformer
Pixel array of CNN
Patch sequence of Vision Transformer

(a) Effect of pooling layer.

(b) Size of receptive field.

(c) Pixel-wise and patch-wise process.

Figure 2: Comparison of CNN and ViT operation from various perspectives.

As organized in figure 2, the above operation of ViT with PSL has the following fundamental characteristics compared to that with CNN, consequently highlighting the need for additional solutions.

1) Absence of Pooling Layer: While CNN contains a pooling layer, ViT often skips the pooling layer except in cases like pooling-based ViT (PiT) Heo et al. (2021b). Due to this difference, ViT not only has less distortion of the hidden representation, but also its size is the same as that of the input, causing a significant amount of privacy leakage as well as communication payload size. On the bright side, this makes regularization on hidden representations more fruitful, just like regularization on input data.

2) Receptive Field Size: A CNN with a convolutional layer is specialized in catching local spatial information of an image, in other words, its receptive field size is small. Conversely, the receptive field of ViT is large enough to learn global spatial information, with the help of its self-attention mechanism. Because of this, ViT is more suitable for producing generalized models compared to CNN, but large-scale datasets are required to unleash the full potential of ViT due to its low inductive bias Baxter (2000). Data regularization can address this large-scale dataset requirement Steiner et al. (2021). In particular, due to its small receptive field, ViT has robustness against large noise applied to part of the image, such as patch drop or image shuffling Naseer et al. (2021), and is thereby suitable for Cutout DeVries and Taylor (2017) or CutMix regularization.

3) Patch-Wise Processing: When CNN processes all operations such as convolution at pixel-wise, ViT performs patch-wise processing such as dividing and embedding images based on a novel unit named patch, which is a square-shaped collection consisting of multiple pixels. Even the self-attention mechanism, which is the core operation of ViT, also operates at the patch-level, and focuses on identifying spatial relations between these patches. As an extension of this patch-wise ViT operation, we deduce that novel patch-wise regularization can be the key to further improving ViT's performance.

Combining *1)*-*3)* leads to one converged solution, a novel regularization that is a patch-wise variant of Cutout or CutMix applied to the hidden representations of ViT with PSL. Its Cutout or CutMix-like properties can maximize the advantages of ViT mentioned in *1)*, while addressing both privacy leakage problem in terms of the client sending fraction, but not entire, of the smashed data. Also, while providing optimized regularization for the receptive field of ViT in *2)*, it can overcome the poor performance of ViT with an insufficient dataset thanks to its inherent regularization effect. Lastly, as suggested in *3)*, the novel patch-wise

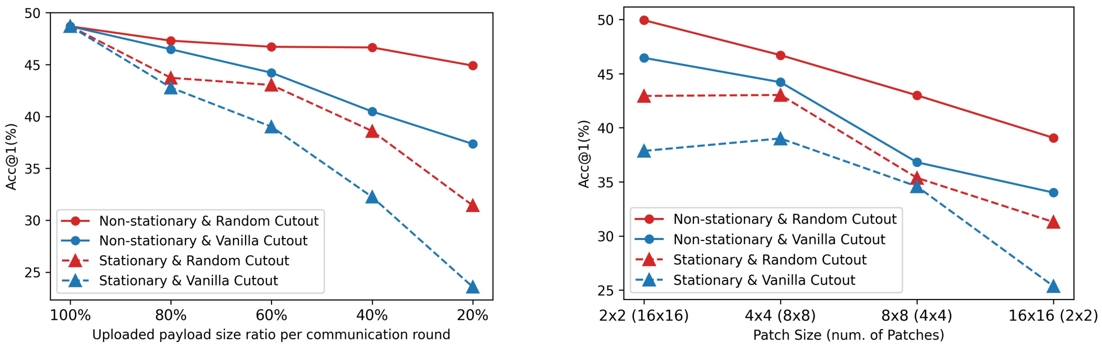

(a) Top-1 Accuracy according to communication cost.

(b) Top-1 accuracy according to patch size.

Figure 3: Accuracy of a single client using Vanilla or Random Cutout whether a mask is stationary or not.

regularization has the potential to suit ViT operation rather than cutting or replacing a box-shaped region consisting of multiple pixels as in a Vanilla Cutout or CutMix.

B Random Cutout at Clients

Departing from the aforementioned potential of the patch-level Cutout or CutMix-like regularization of hidden representations, this subsection first deals with its Cutout-based version, which is also the single-client case of the CutMix-based version. This subsection focuses on its client-side operations, design elements, and properties, and provides insights from them.

Vanilla Cutout. After the patch embedding process, the i-th client of *Vanilla Cutout* DeVries and Taylor (2017) masks out the smashed data as follows:

$$\mathbf{s}_i' = \mathbf{M}_i \odot \mathbf{s}_i, \tag{4}$$

where $\mathbf{M}_i$ is a binary matrix in which the elements belonging to the inside are 0 and the rest are 1 for a random bounding box denoted by $\mathbf{B} = (r_x, r_y, r_w, r_h)$, $\odot$ is an pixel-wise multiplication operator, and $\mathbf{s}_i'$ is called *Cutout smashed data*.

Then, the Cutout smashed data is sent to the server, followed by a server-side FP and BP process of Subsection A, completing a single *communication round* of Vanilla Cutout. At this time, the loss generated by the server is the same as in equation 2, where $f_i(\mathbf{x}_i)$ is replaced with $\mathbf{s}_i'$. This single-client operation is heavily dependent on $\mathbf{M}_i$, but that of Vanilla Cutout is pixel-wise, not patch-wise, requiring an alternative for patchfied ViT.

Random Cutout. Exploring a regularization technique optimized for ViT, we first propose Random Patch-wise Cutout, *Random Cutout* for short. In Random Cutout, $\mathbf{M}_i$ in equation 4 is a patch-wise on-off matrix and is denoted as $\mathbf{M}_i = [\mathbf{M}_{i,0}, \mathbf{M}_{i,1}, \cdots, \mathbf{M}_{i,N}]$, consisting of $\mathbf{M}_{i,j}$ for $j \in \{0, 1, \cdots, N\}$ that is mapped with the corresponding embedded patch $\mathbf{s}_{i,j}$ and determines whether to drop it.

Figure 3 shows that Random Cutout outperforms Vanilla Cutout in terms of top-1 accuracy for all cases. This is consistent with our reasoning that patch-wise regularization would be more suitable for ViT, where all operations are patch-wise. Also, from the point of view of dropout, which is often pointed out as the main reason for the high performance of Vanilla Cutout, it can be similarly inferred that the higher performance of the Random Cutout is rooted in a more dropout-like property (i.e. higher randomness) than Vanilla Cutout. In addition, the Random Cutout includes design elements, as elaborated below.

Impact of Mask Stationarity. For the Random Cutout as well as the Vanilla Cutout, we can divide the cases according to how often $\mathbf{M}_i$ is updated, so in figure 3 we compare the two extreme cases, updated every communication round (non-stationary) or not updated (stationary). Comparing them, the Random or Vanilla Cutout always has high accuracy with the non-stationary mask, which is advantageous for capturing more generalized global spatial information, leading to avoidance of overfitting. In addition, figure 3a shows the accuracy with respect to the communication cost, in other words, the payload size. Here, the uploaded payload size is proportional to the number of 1s among the elements of $\mathbf{M}_i$.For example, the uploaded payload size ratio of 100% means that all elements of $\mathbf{M}_i$ are 1 and the Cutout smashed data is equal to the smashed data. Figure 3a indicates that the top-1 accuracy of both Cutouts decreases as the ratio of uploaded payload size increases, showing the *accuracy and communication cost trade-off*. Among them, Random Cutout with non-stationary mask has the smallest drop in accuracy.

Impact of Patch Size. Regarding patch size, figure 3b demonstrates that the smaller the patch size, the higher the overall accuracy tends to be. Due to the characteristics of the transformer as well as ViT, which learns the relative spatial relationship between patches through positional embedding, small patch size allows for granular and generalized classification.

In summary, we first investigate Random Cutout as well as Vanilla Cutout and scrutinize observations of performance according to mask stationarity or patch size. From here, without further explanation, we use a non-stationary mask and a small patch size (2×2), along with the proposed and baselines.

C Random CutMix at the Server

In this subsection, we propose a *Random Patch-wise CutMix (Random CutMix)* by expanding the Random Cutout to a multi-client scenario. Before explaining the details of Random CutMix's operation, a novel entity called mixer is introduced on the existing network consisting of server and client. While the server is *honest-but-curious*, the mixer is a trusted third party, so key operations of Random CutMix can be performed without privacy leakage. For the mixer, the concept of homomorphic encryption can be applied Rivest et al. (1978); Pereteanu et al. (2022). With homomorphic encryption, computation can be processed under privacy preservation, as the client transmits homomorphically encrypted Cutout smashed data, and the server subsequently produces encrypted output as a mixer. Alternatively, the mixer can be an additional entity such as a mobile network operator or vendor, or an analog channel as in Koda et al. (2021).

Let $\mathbb{C}_k$ be a set of client pairs obtained by non-restored extraction of k clients from the client set $\mathbb{C}$, and define its elements as *mixing groups*. For instance, when $\mathbb{C} = \{1, 2, 3, 4\}$, $\mathbb{C}_2 = \{\{1, 2\}, \{3, 4\}\}$. Inspired by subsection B, where the non-stationary mask performs well, mixing groups are generated in a round-robin manner for each communication round.

Pseudorandom Binary Sequence Generation in Mixer. When performing a Random CutMix, there should be no or minimal overlap between masks to maximize client-side communication efficiency, while no empty patches should exist after aggregation for high accuracy as inferred from figure 3a. Taken together, in order to ensure both accuracy and communication efficiency, the binary masks of clients belonging to identical mixing groups should be MECE in Random CutMix. Specifically, to enable this, for the i-th client in the mixing group $\{1, \cdots, k\}$, the mixer first calculates the i-th *mixing ratio* λ_i following the symmetric dirichlet distribution Bishop et al. (2007) with *mask distribution* α_M. Then, for the i-th client, the mixer extracts $\lceil \lambda_i \cdot N \rceil$ elements from the set $\{1, \cdots, N\}$ without replacement to generate a mask $\mathbf{M}_i$, which allocates the total N patches to k clients without overlapping. For tractability we assume $k = 2$ in the following equations.

Random CutMix. After the mixer sends $\mathbf{M}_i$ to the i-th client, each i-th client produces Cutout smashed data based on its corresponding mask $\mathbf{M}_i$ as in equation 4. First, according to the Gaussian mechanism, each client injects noise into the smashed data and labels as follows:

$$\bar{\mathbf{s}}_i = \mathbf{s}_i + n_{s,i}, \qquad \bar{\mathbf{y}}_i = \mathbf{y}_i + n_{y,i}, \tag{5}$$

where $n_{s,i}$ and $n_{y,i}$ are matrices of size D_s and D_y, and their elements follow a zero-mean Gaussian distribution with variances σ_s^2 and σ_y^2, respectively. Then, each client produces *DP-Cutout smashed data* through the corresponding mask as shown below and returns $(\bar{\mathbf{s}}'_i, \bar{\mathbf{y}}'_i)$ to the mixer:

$$\bar{\mathbf{s}}'_i = \mathbf{M}_i \odot \bar{\mathbf{s}}_i, \qquad \bar{\mathbf{y}}'_i = \lambda_i \cdot \bar{\mathbf{y}}_i. \tag{6}$$

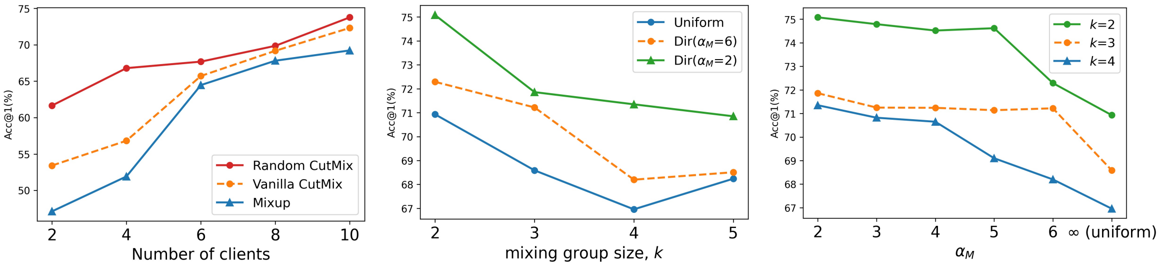

(a) Impact of mixing methods. (b) Impact of mixing group size. (c) Impact of mask distributions (α_M).

Figure 4: Top-1 accuracy of multi-client scenario: (a) accuracy of Random CutMix, Vanilla CutMix, and Mixup w.r.t the number of clients; (b) accuracy of Random CutMix w.r.t the mixing group size; (c) accuracy of Random CutMix w.r.t the mask distribution α_M.

Next, for $\{i, i'\} \in \mathbb{C}_2$ (a set of mixing groups with $k = 2$), the mixer yields *DP-CutMix smashed data* $\tilde{\mathbf{s}}_{\{i,i'\}}$ through Mixup between DP-Cutout smashed data as follows :

$$\tilde{\mathbf{s}}_{\{i,i'\}} = \bar{\mathbf{s}}'_i + \bar{\mathbf{s}}'_{i'}, \qquad \tilde{\mathbf{y}}_{\{i,i'\}} = \bar{\mathbf{y}}'_i + \bar{\mathbf{y}}'_{i'}. \tag{7}$$

The mixer uploads this DP-CutMix smashed data and its label to the server, followed by the server propagates it to the upper model segment to produce the loss of the following formula:

$$\tilde{L}_{\{i,i'\}} = \frac{1}{b}\sum CE(g(\tilde{\mathbf{s}}_{\{i,i'\}}), \tilde{\mathbf{y}}_{\{i,i'\}}), \tag{8}$$

which is the counterpart of equation 2.

The operation up to this point is performed in parallel to other mixing groups in $\mathbb{C}_2$. When the mixer receives cut-layer gradient $\nabla_{\tilde{\mathbf{s}}_{\{i,i'\}}}\tilde{L}_{\{i,i'\}}$ from the server in BP, the effect of the FP flow interrupted by mutually exclusive masks should be reflected in the gradient of each client before it is sent to them. For this, the mixer divides the cut-layer gradient into the gradient of the i-th client and the gradient of the i'-th client as follows:

$$\begin{aligned}\nabla_{\tilde{\mathbf{s}}_{\{i,i'\}}}\tilde{L}_{\{i,i'\}} &= \mathbf{M}_i \odot \nabla_{\tilde{\mathbf{s}}_{\{i,i'\}}}\tilde{L}_{\{i,i'\}} + \mathbf{M}_{i'} \odot \nabla_{\tilde{\mathbf{s}}_{\{i,i'\}}}\tilde{L}_{\{i,i'\}} & (9)\\ &= \underbrace{\nabla_{\tilde{\mathbf{s}}_{\{i,i'\}}}(\mathbf{M}_i \odot \tilde{L}_{\{i,i'\}})}_{\text{gradient for client } i} + \underbrace{\nabla_{\tilde{\mathbf{s}}_{\{i,i'\}}}(\mathbf{M}_{i'} \odot \tilde{L}_{\{i,i'\}})}_{\text{gradient for client } i'}. & (10)\end{aligned}$$

Note that since $\mathbf{M}_{i(i')}$ is a binary matrix, all elements are constants of 0 or 1, and the derivation from equation 9 to equation 10 is trivial by the constant multiply rule of derivate.

After the mixer transmits each gradient to the corresponding client, the weight update of the $i(i')$-th client and server through the BP is available as shown below:

$$\begin{bmatrix}\mathbf{w}_s\\ \mathbf{w}_{c,i(i')}\end{bmatrix} \leftarrow \begin{bmatrix}\mathbf{w}_s\\ \mathbf{w}_{c,i(i')}\end{bmatrix} - \eta\begin{bmatrix}\sum_{\{i,i'\}\in\mathbb{C}_2}(d_i + d_{i'})\cdot(\nabla_{\mathbf{w}_s}\tilde{L}_{\{i,i'\}})\\ \nabla_{\mathbf{w}_{c,i(i')}}\mathbf{M}_{i(i')} \odot \tilde{L}_{\{i,i'\}}\end{bmatrix}. \tag{11}$$

This completes DP-CutMixSL's single communication round. As shown in figure 4, the proposed Random CutMix includes the following design elements.

Random CutMix vs. Vanilla CutMix and Mixup. While the proposed Random CutMix is a patch-wise partial regularization scheme rooted in masking, a Mixup Zhang et al. (2017); Verma et al. (2019) that superpositions the full image can be considered as an alternative. When Mixup is applied instead of Random CutMix, equation 7 is replaced with the following formula: $\hat{\mathbf{s}}_{\{i,i'\}} = \lambda_i \cdot \mathbf{s}_i + \lambda_{i'} \cdot \mathbf{s}_{i'}$, $\hat{\mathbf{y}}_{\{i,i'\}} = \lambda_i \cdot \mathbf{y}_i + \lambda_{i'} \cdot \mathbf{y}_{i'}$. Another alternative is Vanilla CutMix, a masking type regularization equal to Random CutMix. In this case, equation 7 remains the same, but while Random CutMix randomly replaces patches, Vanilla CutMix replaces internal pixels based on the box-shape region as in Vanilla Cutout. Figure 4a shows the comparison

Algorithm 1 Operation of DP-CutMixSL with $k = 2$.

```
Input: mask distribution $\alpha_M$
  /*Execute in mixer*/
  function 1. PSEUDORANDOM SEQUENCE GENERATION
    Generate $\mathbb{C}_2$ by repeating extraction without replacement of 2 clients from client set $\mathbb{C}$
    Sample $\{\lambda_1, .., \lambda_k\} \sim \text{Dir}(\alpha_M)$
    Generate binary masks $\{\mathbf{M}_1, .., \mathbf{M}_k\}$ according to $\{\lambda_1, .., \lambda_k\}$
    Return $\mathbf{M}_i$ to $i$-th client for all $i \in \mathbb{C}_k$
  function 2. RANDOM CUTMIX
    Generate $\{\tilde{\mathbf{s}}_{\{i,i'\}}, \tilde{\mathbf{y}}_{\{i,i'\}}\}$ through equation 7
    Return $\{\tilde{\mathbf{s}}_{\{i,i'\}}, \tilde{\mathbf{y}}_{\{i,i'\}}\}$ to server
  function 3. CUT-LAYER GRADIENT SPLITTING
    Split $\nabla_{\tilde{\mathbf{s}}_{\{i,i'\}}} \tilde{L}_{\{i,i'\}}$ into $\nabla_{\tilde{\mathbf{s}}_{\{i,i'\}}} \mathbf{M}_i \odot \tilde{L}_{\{i,i'\}}$ and $\nabla_{\tilde{\mathbf{s}}_{\{i,i'\}}} \mathbf{M}_{i'} \odot \tilde{L}_{\{i,i'\}}$ through equation 10
    Return $\nabla_{\tilde{\mathbf{s}}_{\{i,i'\}}} \mathbf{M}_{i(i')} \odot \tilde{L}_{\{i,i'\}}$ to $i(i')$-th client

  while $\mathbf{w}_i$ not converged do
    PSEUDORANDOM SEQUENCE GENERATION
    /*Execute in client $i \in \mathbb{C}_k$*/
    Generate $\mathbf{s}_i$ through equation 1
    Generate $(\bar{\mathbf{s}}_i, \bar{\mathbf{y}}_i)$ by applying Gaussian mechanism as in equation 5
    Generate $(\bar{\mathbf{s}}'_i, \bar{\mathbf{y}}'_i)$ through equation 6 using $\mathbf{M}_i$
    Send $(\bar{\mathbf{s}}'_i, \bar{\mathbf{y}}'_i)$ to mixer
    RANDOM CUTMIX
    /*Execute in server
    Generate loss $\tilde{L}_{\{i,i'\}}$ through server-side FP in equation 8
    Update $\mathbf{w}_s$ through equation 11
    Send $\nabla_{\tilde{\mathbf{s}}_{\{i,i'\}}} \tilde{L}_{\{i,i'\}}$ to mixer
    CUT-LAYER GRADIENT SPLITTING
    /*Execute in client $i \in \mathbb{C}_k$*/
    Update $\mathbf{w}_{c,i}$ through equation 11
  end while
```

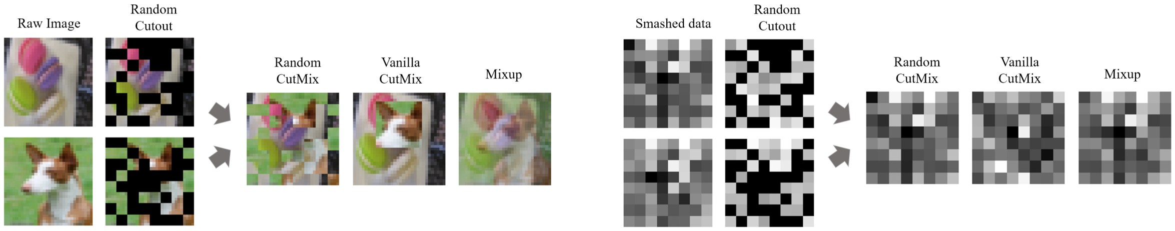

(a) Raw data.

(b) Smashed data.

Figure 5: Examples of image representation applying various image processing techniques to (a) raw data and (b) smashed data.

of accuracy between these regularization schemes according to the number of clients n. The top-1 accuracy is high in the order of Random CutMix, Vanilla CutMix, and Mixup regardless of the number of clients, showing superiority of Random CutMix in ViT. Also, in all three regularization schemes, accuracy increases as the number of clients increases, that is, scalability is guaranteed up to 10 clients. Additionally, figure 5 illustrates the visualization of the output images generated when each regularization scheme is applied to smashed data as well as input data. More image visualizations of this kind are available in appendix B.

Impacts of Mixing Group Size and Mask Distributions. In figure 4b, the accuracy of the Random CutMix as the mixing group size varies is shown for mask distribution α_M. Note here that the infinite divergence of α_M implies that the mixing ratio follows a uniform distribution. Without cases where k is 4 with α_M of 2 or 6, the top-1 accuracy tends to be inversely proportional to the mixing group size, especially its decline is greatest when k changes from 2 to 3. Interpreting this from the perspective of each client, as the mixing group size k increases, large noise that may lead to performance degradation is applied in the remaining areas except for $\frac{1}{k}$ of the entire image, under the assumption of a uniform mixing ratio. For similar reasons regarding distortion level, figure 4c includes a tendency for accuracy to decrease as α_M increases. Based on figure 4, hereafter a Random CutMix in which k and α_M are both equal to 2 is used without further explanation.

In short, in this section, we review the SL framework, and then propose DP-CutMixSL, which combines it with the novel regularization scheme, coined Random CutMix, optimized for the characteristics of ViT. Also, the design elements of DP-CutMixSL are explored, with optimal hyperparameter settings particularly related to its accuracy or communication-efficiency. The detailed operation of the DP-CutMixSL aided by the core functions of mixer is summarized in algorithm 1. Here, although core functions such as Random CutMix and cut-layer gradient splitting are described only for $k = 2$, they are trivially generalizable for $k > 2$. While controlling the mixing group size only in this work, it is possible to increase the number of FP flows by combinatorily setting the mixing group several times during single FP as in Oh et al. (2022b), focusing on its augmentation properties. This can be a solution to the low inductive bias of ViT, which is deferred to future research. In addition, as in Oh et al. (2022a), under the implicit premise of sharing the mask using the seed concept, mixer's functions can be distributed to clients and server, allowing asynchronous training of DP-CutMixSL.

4 Differential Privacy Analysis on Smashed Data

In this section, we theoretically analyze the differential privacy (DP) bound of DP-CutMixSL and validate its effectiveness for privacy guarantees. Unlike existing DP works that focus on the privacy guarantees of samples and labels, we conduct DP analysis from the perspective of smashed data, which is highly correlated with the sample particularly in ViT, and its labels. This is in the same context as analyzing the privacy leakage of model parameters or gradient in FL.

Given the ViT's patch size of P, a dataset $\mathcal{D} = \{(\mathbf{s}_1, \mathbf{y}_1), .., (\mathbf{s}_n, \mathbf{y}_n)\}$ consists of n clients' pairs of smashed data $\mathbf{s}_i \in \mathbb{R}^{P^2 \times N \times C} = \mathbb{R}^{D_s}$ and the corresponding label $\mathbf{y}_i \in \mathbb{R}^L = \mathbb{R}^{D_y}$ is a one-hot vector of size L, where N and C denote the number of patches and channels, respectively. For the sake of convenience, we assume that $\mathbf{s}_i$ and $\mathbf{y}_i$ are normalized so that $\mathbf{s}_i \in [0, \Delta]^{D_s}$ and $\mathbf{y}_i \in [0, 1]^{D_y}$, respectively. Before going further, the definition of Central DP (CDP) Dwork et al. (2006) is organized as follows:

Definition 1 ((ε,δ)-CDP)**.** *For $\varepsilon \geq 0$ and $\delta > 0$, we say that a randomized mechanism $\mathcal{M} : \mathcal{D} \to \mathcal{R}$ is (ε, δ)-CDP if it satisfies the following inequality for any adjacent $D, D' \in \mathcal{D}$ and $U \subset \mathcal{R}$:*

$$Pr[\mathcal{M}(D) \in U] \leq e^{\varepsilon} \cdot Pr[\mathcal{M}(D')] \in U] + \delta, \tag{12}$$

At this point, a small ε indicates a high privacy level implying that one cannot distinguish whether D or D' is used to produce an outcome of mechanism. Although CDP is widely used when analyzing Gaussian mechanisms, we also use the Reńyi DP (RDP) Mironov (2017), defined below, given the tractable interpretation of its composition rule:

Definition 2 ((α, ϵ)-RDP)**.** *A randomized mechanism $\mathcal{M} : \mathcal{D} \to \mathcal{R}$ is said to have ϵ-RDP of order α, or (α, ϵ)-RDP for short, if for any adjacent $D, D' \in \mathcal{D}$ it holds that:*

$$D_\alpha(\mathcal{M}(D)||\mathcal{M}(D')) \leq \epsilon. \tag{13}$$

In addition, Mironov (2017) proves that every RDP mechanism is also (ε, δ)-CDP. Especially in Mironov (2017), when the mechanism is (α, ϵ)-RDP, then it is $(\epsilon + \frac{\log(1/\delta)}{\alpha - 1}, \delta)$-DP for $0 < \delta < 1$. For convenience, this section derives the RDP guarantee and the simulations in the next section measure the CDP guarantee.

A Main Result

Here, we compare the RDP bound of the DP-CutMixSL with that of the SL with Gaussian mechanism *(DP-SL)* as well as that of the case with a Mixup added to it *(DP-MixSL)*.

The first mechanism DP-SL, denoted $\mathcal{M}_1$, is the baseline that applies Gaussian mechanism to smashed data $\mathbf{s}_i$ as well as its corresponding label $\mathbf{y}_i$. Then, the outputs of $\mathcal{M}_1$ are as follows:

$$\bar{\mathbf{s}}_i = \mathbf{s}_i + n_{s,i}, \qquad \bar{\mathbf{y}}_i = \mathbf{y}_i + n_{y,i}, \tag{14}$$

where $n_{s,i} \sim \mathcal{N}(0, \sigma_s^2 I_{D_s})$ and $n_{y,i} \sim \mathcal{N}(0, \sigma_y^2 I_{D_y})$ for all i and some (σ_s, σ_y).

Mechanism $\mathcal{M}_2$ for DP-MixSL takes Mixup first via mixer, followed by Gaussian mechanism $\mathcal{M}_1$, and its output along with the mixing ratio λ_i is denoted as:

$$\hat{\mathbf{s}} = \sum_{i=1}^{n} (\lambda_i \cdot \mathbf{s}_i) + \hat{n}_s, \qquad \hat{\mathbf{y}} = \sum_{i=1}^{n} (\lambda_i \cdot \mathbf{y}_i) + \hat{n}_y, \tag{15}$$

where $\hat{n}_s$ and $\hat{n}_y$ follow $\mathcal{N}(0, \sigma_s^2 I_{D_s})$ and $\mathcal{N}(0, \sigma_y^2 I_{D_y})$ respectively, and $\sum_{i=1}^{n} \lambda_i = 1$.

Lastly, mechanism $\mathcal{M}_3$ executes Random CutMix, then proceeds with Gaussian mechanism $\mathcal{M}_1$. Here, the outputs of $\mathcal{M}_3$, DP-CutMix smashed data and its label, are as follows:

$$\tilde{\mathbf{s}} = \sum_{i=1}^{n} (\mathbf{M}_i \odot \mathbf{s}_i) + \tilde{n}_s, \qquad \tilde{\mathbf{y}} = \sum_{i=1}^{n} (\lambda_i \cdot \mathbf{y}_i) + \tilde{n}_y, \tag{16}$$

where $\mathbf{M}_i$ are MECE binary masks with $N_i = \lceil \lambda_i \cdot N \rceil$ number of non-zero patches for all i, $\tilde{n}_s \sim \mathcal{N}(0, \sigma_s^2 I_{D_s})$, and $\tilde{n}_y \sim \mathcal{N}(0, \sigma_y^2 I_{D_y})$. Note that the operations of $\mathcal{M}_3$ and $\mathcal{M}_2$ are equivalent in terms of labels.

Then, we can measure the RDP bound of DP-CutMixSL, compared to that of DP-SL and DP-MixSL as follows:

Theorem 1. *For a given order $\alpha \geq 2$, the RDP privacy budgets $\epsilon_1(\alpha)$, $\epsilon_2(\alpha)$, and $\epsilon_3(\alpha)$ of DP-SL, DP-MixSL and DP-CutMixSL satisfy the following inequality:*

$$\epsilon_2(\alpha) \leq \epsilon_3(\alpha) \leq \epsilon_1(\alpha), \tag{17}$$

where

$$\epsilon_1(\alpha) = \epsilon_{1,s}(\alpha) + \epsilon_{1,y}(\alpha), \tag{18}$$

$$\epsilon_2(\alpha) = {\lambda_{max}}^2(\epsilon_{1,s}(\alpha) + \epsilon_{1,y}(\alpha)), \tag{19}$$

$$\epsilon_3(\alpha) = \lambda_{max}(\epsilon_{1,s}(\alpha) + \lambda_{max} \cdot \epsilon_{1,y}(\alpha)), \tag{20}$$

in which $\epsilon_{1,s}(\alpha) = \frac{\alpha \Delta^2 D_s}{2\sigma_s^2}$, $\epsilon_{1,y}(\alpha) = \frac{\alpha D_y}{2\sigma_y^2}$, and $\lambda_{max} = \max_{i \in \mathbb{C}} \lambda_i$.

Theorem 1 provides the following 4 observations about DP-CutMixSL.

Privacy-Accuracy Trade-Off ($k = n$). There are 2 major *privacy-accuracy trade-off* with theorem 1. On the one hand, the RDP guarantee of DP-CutMixSL is improved compared to that of DP-SL, but is weaker than that of DP-MixSL, whereas DP-CutMixSL outperforms DP-MixSL in terms of accuracy as will be shown in section 5. In DP-MixSL, a large number of samples are superposed in the entire image (i.e. superposition), but privacy leakage is relatively low because they are blurred, whereas in DP-CutMixSL, although privacy leakage occurs only in a fraction of the image (i.e. masking), the sample is leaked as it is, resulting in a performance gap. Counterintuitively, the accuracy of DP-CutMixSL becomes higher than that of DP-MixSL.

On the other hand, regarding $\lambda_{max} \in [1/n, 1]$, when λ_{max} reaches $1/n$ (i.e. $|\mathbb{C}|$ increases or α_M goes to ∞), the privacy guarantee is maximized and the equality constraint for theorem 1's inequalities is satisfied, but the accuracy decreases as in figure 4b and figure 4c, leading to another privacy-accuracy trade-off.

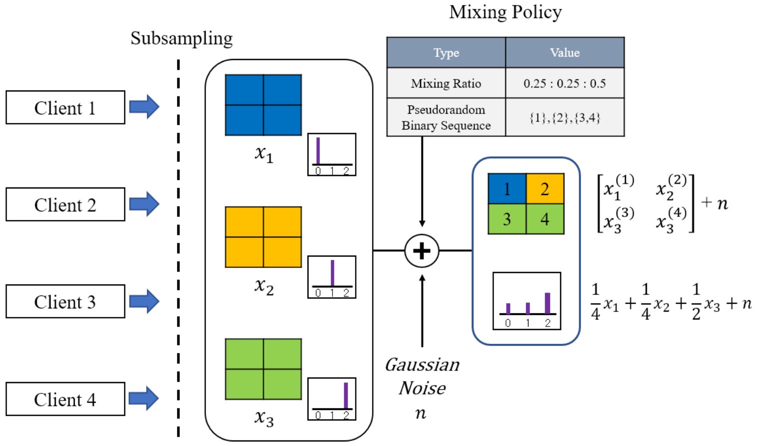

Type	Value
Mixing Ratio	0.25 : 0.25 : 0.5
Pseudorandom Binary Sequence	{1},{2},{3,4}

Mixing Policy
Subsampling
Client 1
Client 2
Client 3
Client 4
x_1
x_2
x_3
0 1 2
Gaussian Noise n
1 2 3 4
$\begin{bmatrix} x_1^{(1)} & x_2^{(2)} \\ x_3^{(3)} & x_3^{(4)} \end{bmatrix} + n$
$\frac{1}{4}x_1 + \frac{1}{4}x_2 + \frac{1}{2}x_3 + n$

Figure 6: An illustration of DP-CutMixSL with subsampling when $n = 4$ and $k = 3$.

RDP-CDP Conversion. We can measure the CDP guarantee of DP-CutMixSL by applying the aforementioned RDP-to-CDP conversion to theorem 1, which is based on the RDP guarantee. Additionally, the effect of the mixing group size can be reflected by using the CDP bound formula of the subsampled mechanism in Wang et al. (2019), whereas theorem 1 implicitly assumes that the mixing group size is equal to n. Thereby, for $k < n$, we can derive the CDP guarantee of DP-CutMixSL with subsampling ($\mathcal{M}^3 \circ$ **subsample**) as below, whose key operation consists of 1) a subsampling mechanism that randomly selects k out of a total of n datapoints (reflecting the mixing group size), and 2) operation of $\mathcal{M}^3$ as depicted in figure 6.

Corollary 1. *For all integer $\alpha \geq 2$ and $0 < \delta < 1$, the DP privacy budgets $\varepsilon'_1(\delta)$, $\varepsilon'_2(\delta)$, and $\varepsilon'_3(\delta)$ of $\mathcal{M}^1 \circ$ **subsample**, $\mathcal{M}^2 \circ$ **subsample** and $\mathcal{M}^3 \circ$ **subsample** satisfy the following inequality:*

$$\varepsilon'_2(\delta) \leq \varepsilon'_3(\delta) \leq \varepsilon'_1(\delta), \tag{21}$$

where

$$\varepsilon'_1(\delta) = \log\left(1 + \frac{k}{n}(e^{\epsilon_1(\alpha)+\varepsilon_o(\delta)} - 1)\right), \tag{22}$$

$$\varepsilon'_2(\delta) = \log\left(1 + \frac{k}{n}(e^{\epsilon_2(\alpha)+\varepsilon_o(\delta)} - 1)\right), \tag{23}$$

$$\varepsilon'_3(\delta) = \log\left(1 + \frac{k}{n}(e^{\epsilon_3(\alpha)+\varepsilon_o(\delta)} - 1)\right), \tag{24}$$

in which $k_2^* = \sqrt{\frac{\epsilon_{1,s}(\alpha)+\epsilon_{1,y}(\alpha)}{\varepsilon_o(\delta)}}$ and $k_3^* = \sqrt{\frac{\epsilon_{1,y}(\alpha)}{\varepsilon_o(\delta)}}$ minimize $\varepsilon'_2(\delta)$ and $\varepsilon'_3(\delta)$ under the assumption that $\lambda_i = 1/k \; \forall i$, respectively, and $\varepsilon_o(\delta) = \frac{\log(1/\delta)}{\alpha-1}$.

Sketch of Proof. *Recall theorem 1, and apply it to the DP bound formula of the subsampled mechanism of Wang et al. (2019) (if $\mathcal{M}$ is (ε, δ)-DP, then the subsampled mechanism $\mathcal{M} \circ$ **subsample** is $(log(1 + \gamma(e^{\varepsilon} - 1)), \gamma\delta)$-DP where γ denotes sampling ratio). This yields equation 21.*

Assuming $\max_{i\in\mathbb{C}} \lambda_i = 1/k$, for $\epsilon_3(\alpha) + \varepsilon_o(\delta) \ll 1$, $\varepsilon'_3(\delta) = \log\left(1 + \frac{k}{n}(e^{\epsilon_3(\alpha)+\varepsilon_o(\delta)} - 1)\right)$ is approximated by $\log\left(1 + \frac{k}{n}(\epsilon_3(\alpha) + \varepsilon_o(\delta))\right)$. Since the log function is a monotone increasing function and n is fixed, $k \cdot (\epsilon_3(\alpha) + \varepsilon_o(\delta))$ should be minimized for the minimum $\varepsilon'_3(\delta)$. Regarding $k \cdot (\epsilon_3(\alpha) + \varepsilon_o(\delta))$, since it is a convex function for $k > 0$, we can find k_3^* which becomes 0 when differentiated. k_2^* can also be calculated in a similar manner. This completes the proof. ■

Revisiting Privacy-Accuracy Trade-Off ($k < n$). First, privacy-accuracy trade-off between DP-MixSL and DP-CutMixSL occurs in corollary 1 as in theorem 1 where $n = k$. The existence of an optimal mixing group size is rooted in subsampling. In the existing Mixup or Random CutMix, the privacy guarantee improves when the number of samples increases, but counterintuitively, with subsampling, the randomness of which client among all clients a specific sample belongs to decreases, resulting in a trade-off.

Limitations on DP Analysis. There are 2 major limitations on our DP analysis. Firstly, in existing DP analysis, it fundamentally measures how sensitively the output changes compared to the input, and at this time, the output is in-practice bounded (for example, classification). However, since SL inherently lacks in quantifying the change of smashed data versus input, we indirectly analyze the privacy guarantee of smashed data versus output. Instead, we experimentally measure the robustness against the reconstruction attack in section 5 to ensure privacy guarantee between input and smashed data.

Secondly, DP analysis cannot differentiate between Random CutMix and Vanilla CutMix because it focuses on the quantity rather than the randomness or pattern of the mechanism. Through the robustness of the reconstruction attack in section 5 mentioned above, we bypass the privacy guarantee between CutMix, which is theoretically indistinguishable.

From the next subsection, the proof of the propositions for deriving theorem 1 follows.

B Proof of Theorem 1: DP-SL Analysis

We now demonstrate the RDP guarantee of DP-SL as follows:

Proposition 1. *For all integer $\alpha \geq 2$, $\mathcal{M}_1$ is $(\alpha, \epsilon_1(\alpha))$-RDP, where*

$$\epsilon_1(\alpha) = \frac{\alpha \Delta^2 D_s}{2\sigma_s^2} + \frac{\alpha D_y}{2\sigma_y^2}. \tag{25}$$

Proof. *Starting from the definition 2 and the Rényi divergence formula with multi-variate Gaussian distributions Gil et al. (2013), the RDP bound of $\mathcal{M}_1$, denoted by $\epsilon_1(\alpha)$, can be expressed as:*

$$\epsilon_1(\alpha) = \sup_{D,D'} D_\alpha(\mathcal{M}_1(D)||\mathcal{M}_1(D')) = \sup_{D,D'} \underbrace{\frac{\alpha \cdot ||\mu_s^D - \mu_s^{D'}||^2}{2\sigma_s^2}}_{=\epsilon_{1,s}(\alpha)} + \underbrace{\frac{\alpha \cdot ||\mu_y^D - \mu_y^{D'}||^2}{2\sigma_y^2}}_{=\epsilon_{1,y}(\alpha)}, \tag{26}$$

since $\bar{\mathbf{s}}_i \sim \mathcal{N}(\mu_s^D, \sigma_s^2 I_{D_s})$ and $\bar{\mathbf{y}}_i \sim \mathcal{N}(\mu_y^D, \sigma_y^2 I_{D_y})$, where μ_s^D and μ_y^D indicate the average of smashed data and that of label, belonging to dataset D. It is noteworthy that $\epsilon_1(\alpha)$ is represented as the sum of RDP bound for smashed data $\epsilon_{1,s}(\alpha)$ and RDP bound for label $\epsilon_{1,y}(\alpha)$ via the sequential composition rule, aiming to induce smashed data-label pairwise RDP bound.

Here, by using assumptions about the pixel-wise upper bound of the smashed data and labels ($\mathbf{s}_i \in [0, \Delta]^{D_s}$ and $\mathbf{y}_i \in [0, 1]^{D_y}$), we have:

$$||\mu_s^D - \mu_s^{D'}||^2 \leq \Delta^2 \cdot D_s, \qquad ||\mu_y^D - \mu_y^{D'}||^2 \leq 1^2 \cdot D_y = D_y. \tag{27}$$

Combining equation 26 and equation 27 concludes the proof. ■

C Proof of Theorem 1: DP-MixSL Analysis

We present the privacy guarantee of DP-MixSL as belows:

Proposition 2. *For all integer $\alpha \geq 2$, $\mathcal{M}_2$ is $(\alpha, \epsilon_2(\alpha))$-RDP, where*

$$\epsilon_2(\alpha) = (\max_{i \in \mathbb{C}} \lambda_i)^2 (\frac{\alpha \Delta^2 D_s}{2\sigma_s^2} + \frac{\alpha D_y}{2\sigma_y^2}). \tag{28}$$

Proof. *Consider the output of DP-MixSL where n smashed data and labels are mixed up, and their pixel-wise upper bound and dimension. Then, for two adjacent datasets D and D' (i.e. only i'-th elements are different, $1 \leq i' \leq n$), we have:*

$$||\mu_s^D - \mu_s^{D'}||^2 \leq (\lambda_{i'} \Delta)^2 D_s, \qquad ||\mu_y^D - \mu_y^{D'}||^2 \leq \lambda_{i'}^2 D_y. \tag{29}$$

Here, equation 29 is maximized when $\lambda_{i'}$ is the maximum value of λ_i for all i. Expressing this is as follows:

$$(\lambda_{i'}\Delta)^2 D_s \leq (\max_{i\in\mathbb{C}} \lambda_i \cdot \Delta)^2 D_s, \qquad \lambda_{i'}^2 D_y \leq (\max_{i\in\mathbb{C}} \lambda_i)^2 D_y. \tag{30}$$

Recalling the Rényi divergence formula and combining it with equation 30 completes the proof. ■

D Proof of Theorem 1: DP-CutMixSL Analysis

The following privacy guarantee of DP-CutMixSL is induced:

Proposition 3. *For all integer $\alpha \geq 2$, $\mathcal{M}_3$ is $(\delta, \epsilon_3(\alpha))$-RDP, where*

$$\epsilon_3(\alpha) = (\max_{i\in\mathbb{C}} \lambda_i) \cdot (\frac{\alpha\Delta^2 D_s}{2\sigma_s^2} + (\max_{i\in\mathbb{C}} \lambda_i)\frac{\alpha D_y}{2\sigma_y^2}). \tag{31}$$

Proof. *If we consider the mean of $\tilde{\mathbf{s}}$ for two adjacent datasets D and D', where only the i'-th element is different, $N_{i'}P^2C$ pixels among the total D_s pixels are different and the rest are identical. At this time, considering the upper bound of the pixel-level, the following inequality is established:*

$$||\mu_s^D - \mu_s^{D'}||^2 \leq (N_{i'}P^2C)\Delta^2 = (\lambda_{i'}NP^2C)\Delta^2 = \lambda_{i'}\Delta^2 D_s. \tag{32}$$

When $\lambda_{i'} = \max_{i\in\mathbb{C}} \lambda_i$, that is to say, $N_{i'} = \max_{i\in\mathbb{C}} N_i$, equation 32 is maximized as follows:

$$\begin{aligned} ||\mu_s^D - \mu_s^{D'}||^2 &\leq (\max_{i\in\mathbb{C}} \lambda_i)\Delta^2 D_s & (33)\\ &= (\max_{i\in\mathbb{C}} N_i)P^2C\Delta^2. & (34)\end{aligned}$$

Recall the Rényi divergence formula, and substitute equation 34 to obtain a privacy guarantee for DP-CutMix smashed data. Since $\mathcal{M}_3$ is identical to $\mathcal{M}_2$ in terms of labels, the proof is completed by applying this to the RDP sequential composition rule together with $\mathcal{M}_2$'s label privacy guarantee. ■

In summary, this section derives the DP bound of the proposed DP-CutMixSL and theoretically demonstrates its effectiveness in terms of amplifying the DP guarantee.

5 Numerical Evaluation

While section 4 theoretically demonstrates the privacy guarantee of DP-CutMixSL, this section experimentally analyzes its privacy guarantee, accuracy, and communication efficiency compared to PSL, SFL Thapa et al. (2020b), and etc. For the experiment, we use the CIFAR-10 dataset Krizhevsky (2009) with a batch size of 128, and table 3 additionally uses the Fashion-MNIST dataset Xiao et al. (2017). As an optimizer, Adam with decoupled weight decay (AdamW) Loshchilov and Hutter (2017) is used with a learning rate of 0.001, and a total of 10 clients each have 5,000 images. Except for table 3, we use the ViT-tiny Touvron et al. (2020) model, and the entire model is split so that the client and server each have an embedding layer and a transformer. Other parameters for DP measurement are in table 1 and a list of notations is available in appendix A.

A Privacy Analysis: Robustness Against Membership Inference/Reconstruction/Label Inference Attacks

We first divide the privacy analysis into robustness against three types of privacy attacks: membership inference attack, reconstruction attack, and label inference attack. Regarding the membership inference attack and the reconstruction attack, an honest-but-curious server attemps to determine whether specific input data was used for learning or to restore input data through an auxiliary network, respectively, from the smashed data of FP. In the label inference attack, a client attempts to infer the label of input data used by other clients for learning from the gradient of BP.

Table 1: Parameters for DP measurement.

Parameter	Annotation	Value
Number of clients	n	10
Number of patches	$N = HW/P^2$	64
Patch size	P	2×2
Dimension of smashed data	D_s	10
Dimension of label	$D_y = L$	2
Pixel-wise upper bound of smashed data	Δ	0.15
Mixing ratio	$\lambda_i \ \forall i$	$1/k$ (uniform)
RDP parameter	α	2
DP parameter	δ	0.5
Noise variance	σ_s^2, σ_y^2	{8/255, 16/255, 32/255}

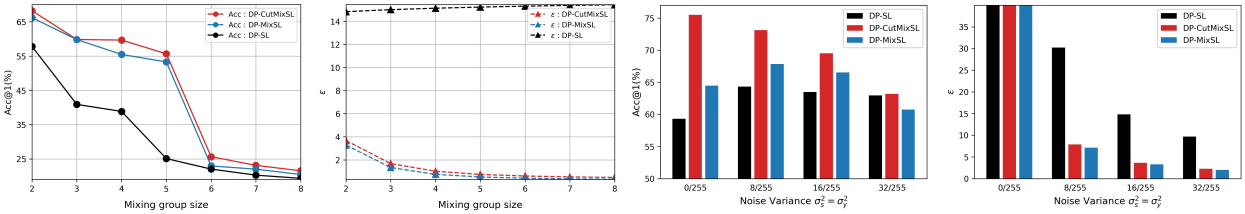

(a) Acc w.r.t k.

(b) ε w.r.t k.

(c) Acc w.r.t σ_s^2 and σ_y^2.

(d) ε w.r.t σ_s^2 and σ_y^2.

Figure 7: Top-1 accuracy and ε under the CIFAR-10 dataset: (a) accuracy of DP-CutMixSL and DP-MixSL according to the mixing group size; (b) ε of DP-CutMixSL and DP-MixSL according to the mixing group size; (c) accuracy of DP-CutMixSL, DP-SL, and DP-MixSL according to noise variance; (d) ε of DP-CutMixSL, DP-SL, and DP-MixSL according to noise variance.

Privacy Against Membership Inference Attacks. Here, assuming the worst case where the server knows the dataset of each client, note that the DP guarantee in section 4 is equivalent to the privacy guarantee for membership inference attack, in that the use of the dataset is inferred through the output.

First, figure 7a and figure 7b shows the effect of mixing group size on accuracy and DP guarantee (ε) of DP-CutMixSL, DP-MixSL, and DP-SL. The first thing to note is the strong privacy guarantee of DP-CutMixSL compared to DP-SL. Factors that improve the DP guarantee of DP-CutMixSL include 1) noise injected by Gaussian mechanism and 2) DP guarantee amplification through Random CutMix, and such gap in privacy guarantee between DP-SL and DP-CutMixSL shows that the latter is more critical to privacy.

Compared to DP-MixSL, regardless of the mixing group size, DP-CutMixSL has higher accuracy compromising a negligible privacy guarantee. Both accuracy and ε of DP-CutMixSL and DP-MixSL decrease as the mixing group size increases, while those of DP-SL tend to be reversed. This is because in the trade-off of privacy guarantee between subsampling and CutMix or Mixup, the privacy guarantee gain of CutMix or Mixup as k increased is greater than the loss of privacy guarantee due to subsampling, resulting in a "Hiding in the crowd" effect Jeong et al. (2020). It can also be explained by how large the optimal mixing group size is (convex function with respect to k), and large k_2^* as well as k_3^* for given parameters validate it ($k_2^* = 28.55$, $k_3^* = 27.07$). On the other hand, DP-SL lacks CutMix or Mixup, so a small k leads to a strong privacy guarantee due to subsampling. Regarding the tendency of accuracy, as shown in figure 4b, the decrease in accuracy for mixing group size is explainable by large-scale noise that is applied to a larger fraction of the image. Furthermore, both DP-CutMixSL and DP-MixSL maintain accuracy until the mixing group size is 5 while improving privacy guarantee.

Figure 7c and figure 7d show accuracy and ε according to noise variance, respectively. Compared to DP-SL and DP-MixSL, DP-CutMixSL achieves the highest accuracy for all noise variances, while ε of DP-MixSL is slightly lower than that of DP-CutMixSL. Hereafter, we measure performance on noiseless environments and rename the techniques accordingly, DP-CutMixSL as CutMixSL, DP-MixSL as PSL w. Mixup, etc.

	Training Dataset (10%)				Training Dataset (100%)			
	Mask Distribution (α_M)				Mask Distribution (α_M)			
	2		6		2		6	
mixing group size (k)	2	4	2	4	2	4	2	4
PSL	0.403	0.425	0.326	1.425	0.116	0.308	0.138	0.398
PSL w. Mixup	**0.665**	0.383	0.379	**1.923**	0.172	0.396	0.215	0.292
PSL w. Patch Cutout	0.415	0.439	0.358	1.352	0.153	0.295	0.187	0.423
PSL w. Vanilla CutMix	0.382	0.426	0.429	1.316	0.180	**0.403**	0.219	0.417
CutMixSL (proposed)	0.425	**0.466**	**0.441**	1.561	**0.187**	0.312	**0.221**	**0.435**

Table 2: Reconstruction loss (MSE) of SL-based techniques according to mixing group size, train dataset size, and mask distribution.

Privacy Against Reconstruction Attacks. Table 2 shows the reconstruction loss of SL-based methods according to various hyperparameters. For reconstruction attack, an auxiliary network is used that takes smashed data as input and produces *restored data* through two convolutional layers and interpolate as output. Then, the auxiliary network is trained by minimizing the mean-squared-error (MSE) loss between the restored data and the input data, to generated restored data with high mutual information between the input data. Regarding the hyperparameters, we adjust the dataset size for training the auxiliary network, mask distribution, and mixing group size. Also, examples of restored data generated through the auxiliary network are in appendix B.

First, with respect to the overall tendency for hyperparameters, the larger the training dataset size, the smaller the mask distribution, and the smaller the mixing group size, the more advantageous the auxiliary network is to learn the restored data, leading to a small reconstruction loss.

When comparing SL-based techniques, the reconstruction loss of the proposed CutMixSL is the largest, in other words, CutMixSL outperforms in terms of privacy guarantee for reconstruction attack in most cases, followed by PSL w. Mixup. In particular, when comparing CutMixSL (Random CutMix) and PSL w. vanilla CutMix, the robustness of CutMixSL is superior for most hyperparameter settings. This is due to the difference in randomness between Vaniila CutMix and Random CutMix, which is previously indistinguishable by DP analysis. Since adjacent box-shaped pixels are replaced, Vanilla CutMix has a relatively high correlation between pixels, while the correlation between pixels in a Random CutMix that is randomly replaced patch-wise is bounded in patch units, straightforwardly leading to a strong privacy guarantee.

Privacy Against Label Inference Attacks. For label inference attacks, there are white-box attacks in Yang et al. (2022), black-box attacks in Li et al. (2021), and other minor variations. We consider a white-box attack among them, since black-box attacks include the bold assumption that clients know the upper model segment weight of the server. Unlike Li et al. (2021), which is based on Vanilla SL, we consider the following worst case of CutMixSL to enable powerful white-box attacks in parallelized form of SL: 1) the first assumption of weight averaging as in SFL to share the weight of the lower model segment among clients, 2) the second assumption that the gradient in the cut-layer is averaged as in Pal et al. (2021) before broadcasting to clients, 3) the third assumption that label inference leakage occurs between clients within the same mixing group size for CutMixSL with $k = 2$. Also, we refer to CutMixSL as its best case when not with the above assumptions. Then, a honest-but-curious client aims to infer its label by measuring the norm (*norm leak*) or cosine similarity (*cosine leak*) of the averaged cut-layer gradient as well as the gradient propagate to the lower model segment.

For measurement, we compute the *area under the ROC curve (AUC)* over the distribution of the norm or cosine similarity. The ROC curve means the curve of the true positive rate (TPR) and false positive rate (FPR) as the decision boundary moves from $-\infty$ to ∞ in a binary classification scenario, and if its base area, AUC, is close to 1, it means that the classification of the two distributions becomes clear under accurate data

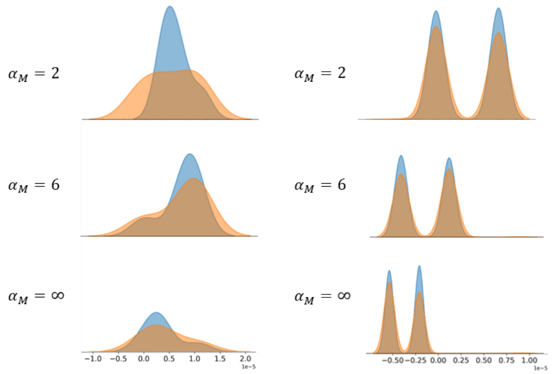

(a) SFL. (b) CutMixSL.

Figure 8: Norm distribution of gradients according to mask distribution.

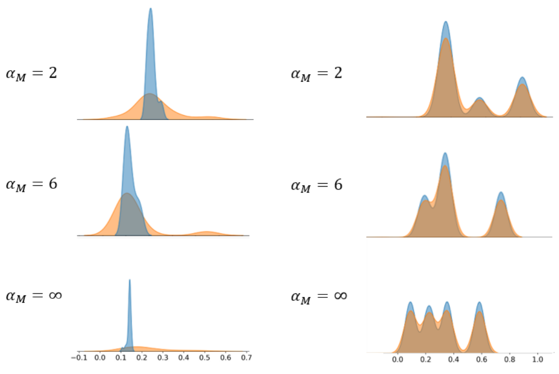

(a) SFL. (b) CutMixSL.

Figure 9: Cosine similarity distribution of gradients according to mask distribution.

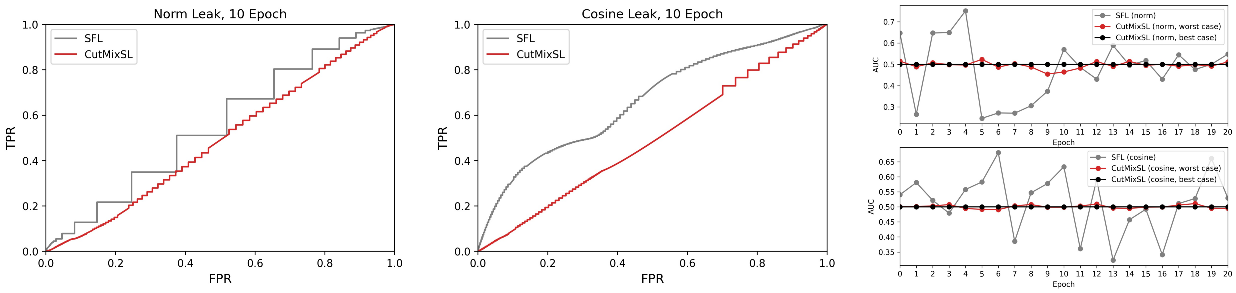

(a) ROC curve of norm leak. (b) ROC curve of cosine leak. (c) AUC of norm and cosine leak.

Figure 10: Privacy guarantee measurement for label inference attack of CutMixSL and SFL.

labeling. Thus, in our scenario, an AUC close to 0.5 implies a high privacy guarantee against label inference attacks. As an experimental setting, we utilize the LeNet-5 model LeCun et al. (2015), where the cut-layer is located after the second convolutional layer, and allocate 1,000 samples each corresponding to the two labels 0 and 4 of MNIST dataset to two clients. As a comparator, we use SFL with cut-layer gradient averaging.

Figure 8 and 9 visualize the distribution of norm and cosine similarity according to the mask distribution of CutMixSL and SFL, respectively. where the orange and blue regions each represent that the labels are positive and negative. We can visually confirm that, as the mask distribution increases, CutMixSL does not change significantly, whereas in SFL, the variance of the distribution increases, making it easier to distinguish. Based on these, the ROC curves for norm leak and cosine leak are shown in figure 10a and 10b.

Further, figure 10c measures AUC per epoch of SFL and CutMixSL (its worst case as well as its best case) for norm and cosine leaks. The first thing to note is the strong privacy guarantee for norm and cosine leak of CutMixSL for both cases, maintaining an AUC close to 0.5 for all epochs, thanks to parallelization and Random CutMix's masking effect on gradient of equation 10. The baseline SFL reaches AUCs up to 0.75 and 0.68 for norm and cosine leak, respectively, roughly alleviated by parallelization alone. In addition, regarding the impact of norm and cosine leak according to epoch, the variance of norm leak AUC is larger at the beginning of learning, but becomes weaker as epoch progresses, and instead, the variance of cosine leak AUC becomes large, showing the potential complementary threats of the two privacy attacks.

B Performance Analysis: Accuracy & Communication-Efficiency

In this subsection, we evaluate the performance of CutMixSL by dividing it into accuracy and communication-efficiency. In table 3, we additionally measure the accuracy for PiT-tiny Heo et al. (2021a) and VGG-

Table 3: Top-1 accuracy of methods for various datasets and models.

Method	Models w/ CIFAR-10			Models w/ Fashion-MNIST		
	ViT-Tiny	PiT-Tiny	VGG-16	ViT-Tiny	PiT-Tiny	VGG-16
Standalone	48.84	47.77	54.97	77.65	78.21	80.12
PSL	57.21	52.28	62.62	85.68	82.35	84.39
SFL	67.88	55.63	63.98	89.17	84.27	87.34
PSL w. Mixup	69.23	64.89	**68.20**	88.21	87.62	88.53
PSL w. Random Cutout	53.86	50.28	56.65	88.46	86.48	88.17
PSL w. Vanilla CutMix	71.78	58.21	33.50	87.86	86.31	89.01
CutMixSL (proposed)	**73.77**	**71.26**	67.53	**89.75**	**89.25**	**89.45**

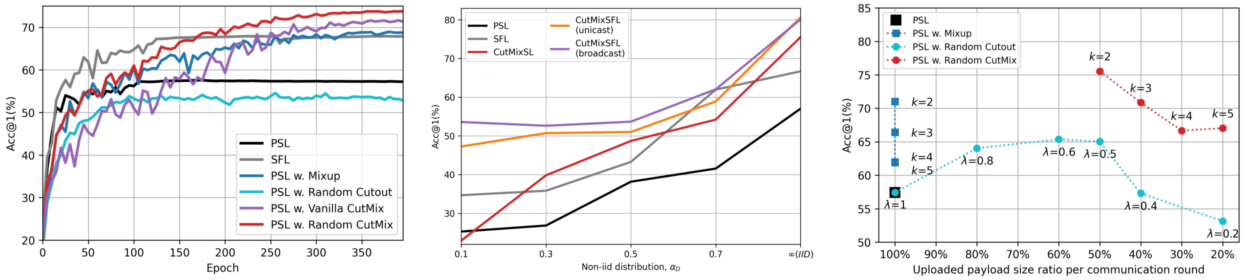

(a) Learning curves.

(b) Acc w.r.t α_D.

(c) Acc-communication effiency.

Figure 11: Performance measurements of SL-based techniques: (a) top-1 accuracy over epoch; (b) top-1 accuracy according to non-IIDness. (c) top-1 accuracy and communication payload size for hyperparameters.

16 Simonyan and Zisserman (2014) except for ViT-tiny. Here, VGG-16 is for CNN in addition to ViT, and PiT is a model between ViT and CNN and is a transformer architecture equipped with a pooling layer.

Accuracy under IID Dataset. Table 3 shows the top-1 accuracy on the CIFAR-10 and Fashion-MNIST datasets of various SL-based techniques, including CutMixSL. First, the accuracy of CutMixSL is the highest in all cases except for the case where VGG-16 and CIFAR-10 are used. With VGG-16 and CIFAR-10, PSL w. Mixup achieves the highest accuracy. This is because, as mentioned earlier, CNN focuses on locality when learning spatial information, while ViT focuses on globality. Also, it is consistent with Naseer et al. (2021), indicating that ViT has robustness of accuracy against patch drop or image shuffling compared to CNN. For that reason, CNN and ViT are better suited for superposition type regularization (i.e., Mixup) and masking type regularization (i.e., Cutout, CutMix), respectively Harris et al. (2020). Compared to PSL w. Vanilla CutMix, CutMixSL is superior in terms of accuracy, which proves the efficiency of the patch-wise designed regularizer in ViT. From the dropout Srivastava et al. (2014) perspective, it can be seen that the more randomized CutMixSL leads to higher accuracy, as in the previous comparison between Vanilla and Random Cutout of figure 3. Furthermore, as in appendix C, Random CutMix achieves the highest accuracy even when applied at the input layer. Lastly, figure 11a contains the learning curves of the corresponding techniques on the CIFAR-10 dataset, showing the superiority of CutMixSL in terms of convergence speed as well as accuracy.

Accuracy under non-IID Dataset. Figure 11b shows the performance of CutMixSL according to the non-IIDness of the dataset α_D. CutMixSL achieves higher accuracy than PSL or SFL, but as non-IIDness becomes more severe (i.e. small α_D), the performance drop is greater. To compensate for this, we design *CutMixSFL*, which introduces lower model aggregation as in Thapa et al. (2020b) and SplitAvg as in Pal et al. (2021). As a result, CutMixSFL maintains high accuracy even at low α_D and records the highest accuracy even under the IID condition with $\alpha_D = 9,999$, while compromising the privacy guarantee as discussed in robustness against label inference attack. This is because the server and client can overcome the biased BP flow through the weight and gradient averaging, which will be discussed in detail in future work.

Another interesting point is that in CutMixSFL, thanks to the help of SplitAvg, the averaged gradient can be sent through broadcasting during BP. For example, as in equation 10, in the existing CutMixSL or CutMixSFL without SplitAvg, the mixer unicasts the i-th masked gradient $\nabla_{\tilde{\mathbf{s}}_{\{i,i'\}}}(\mathbf{M}_i \odot \tilde{L}_{\{i,i'\}})$ to the i-th client, whereas in CutMixSFL with SplitAvg, the server directly broadcasts the averaged gradient to $i(i')$-th client, enabling full band utilization.

Communication Efficiency. Figure 11c shows the corresponding accuracy for the uploaded payload size of various SL-based methods. First, we confirm that the increase in communication efficiency of Random CutMix or Random Cutout as k or λ increases. Meanwhile, Mixup lacks communication efficiency gains due to its inherent superposition of the entire image. Also, when k increases, the accuracy of Random CutMix decreases, resulting in an accuracy-communication efficiency trade-off of Random CutMix.

6 Conclusion

In this study, we designed DP-CutMixSL with the goal of developing a privacy preserving distributed ML algorithm for ViT. Thanks to the randomness and masking effect of Random CutMix, we theoretically and experimentally demonstrated that the proposed DP-CutMixSL has robustness against three types of privacy attacks, while not compromising accuracy or communication-efficiency. Although DP guarantee for smashed data was theoretically derived in FP, but our study lacks it in BP. Combined with GradPerturb in Yang et al. (2022), exploring the DP guarantee at BP could be an interesting topic for future work.

References

Martin Abadi, Andy Chu, Ian Goodfellow, H Brendan McMahan, Ilya Mironov, Kunal Talwar, and Li Zhang. Deep learning with differential privacy. In *Proceedings of the 2016 ACM SIGSAC conference on computer and communications security*, pages 308–318, 2016.

Sihun Baek, Jihong Park, Praneeth Vepakomma, Ramesh Raskar, Mehdi Bennis, and Seong-Lyun Kim. Visual transformer meets cutmix for improved accuracy, communication efficiency, and data privacy in split learning. *arXiv preprint arXiv:2207.00234*, 2022.

Borja Balle, Gilles Barthe, and Marco Gaboardi. Privacy amplification by subsampling: Tight analyses via couplings and divergences. *Advances in Neural Information Processing Systems*, 31, 2018.

Jonathan Baxter. A model of inductive bias learning. *Journal of artificial intelligence research*, 12:149–198, 2000.

Yvonne M Bishop, Stephen E Fienberg, and Paul W Holland. *Discrete multivariate analysis: theory and practice*. Springer Science & Business Media, 2007.

Eitan Borgnia, Jonas Geiping, Valeriia Cherepanova, Liam Fowl, Arjun Gupta, Amin Ghiasi, Furong Huang, Micah Goldblum, and Tom Goldstein. Dp-instahide: Provably defusing poisoning and backdoor attacks with differentially private data augmentations. *arXiv preprint arXiv:2103.02079*, 2021.

Tom Brown, Benjamin Mann, Nick Ryder, Melanie Subbiah, Jared D Kaplan, Prafulla Dhariwal, Arvind Neelakantan, Pranav Shyam, Girish Sastry, Amanda Askell, et al. Language models are few-shot learners. *Advances in neural information processing systems*, 33:1877–1901, 2020.

Nicolas Carion, Francisco Massa, Gabriel Synnaeve, Nicolas Usunier, Alexander Kirillov, and Sergey Zagoruyko. End-to-end object detection with transformers. In *European conference on computer vision*, pages 213–229. Springer, 2020.

Chun-Fu Richard Chen, Quanfu Fan, and Rameswar Panda. Crossvit: Cross-attention multi-scale vision transformer for image classification. In *Proceedings of the IEEE/CVF international conference on computer vision*, pages 357–366, 2021.

Jacob Devlin, Ming-Wei Chang, Kenton Lee, and Kristina Toutanova. Bert: Pre-training of deep bidirectional transformers for language understanding. *arXiv preprint arXiv:1810.04805*, 2018.

Terrance DeVries and Graham W Taylor. Improved regularization of convolutional neural networks with cutout. *arXiv preprint arXiv:1708.04552*, 2017.

Alexey Dosovitskiy, Lucas Beyer, Alexander Kolesnikov, Dirk Weissenborn, Xiaohua Zhai, Thomas Unterthiner, Mostafa Dehghani, Matthias Minderer, Georg Heigold, Sylvain Gelly, Jakob Uszkoreit, and Neil Houlsby. An image is worth 16x16 words: Transformers for image recognition at scale. *CoRR*, abs/2010.11929, 2020a. URL `https://arxiv.org/abs/2010.11929`.

Alexey Dosovitskiy, Lucas Beyer, Alexander Kolesnikov, Dirk Weissenborn, Xiaohua Zhai, Thomas Unterthiner, Mostafa Dehghani, Matthias Minderer, Georg Heigold, Sylvain Gelly, et al. An image is worth 16x16 words: Transformers for image recognition at scale. *arXiv preprint arXiv:2010.11929*, 2020b.

Cynthia Dwork. Differential privacy: A survey of results. In *International conference on theory and applications of models of computation*, pages 1–19. Springer, 2008.

Cynthia Dwork, Krishnaram Kenthapadi, Frank McSherry, Ilya Mironov, and Moni Naor. Our data, ourselves: Privacy via distributed noise generation. In *Annual international conference on the theory and applications of cryptographic techniques*, pages 486–503. Springer, 2006.

Úlfar Erlingsson, Vitaly Feldman, Ilya Mironov, Ananth Raghunathan, Kunal Talwar, and Abhradeep Thakurta. Amplification by shuffling: From local to central differential privacy via anonymity. In *Proceedings of the Thirtieth Annual ACM-SIAM Symposium on Discrete Algorithms*, pages 2468–2479. SIAM, 2019.

Yansong Gao, Minki Kim, Sharif Abuadbba, Yeonjae Kim, Chandra Thapa, Kyuyeon Kim, Seyit A Camtepe, Hyoungshick Kim, and Surya Nepal. End-to-end evaluation of federated learning and split learning for internet of things. *arXiv preprint arXiv:2003.13376*, 2020.

Yansong Gao, Minki Kim, Chandra Thapa, Sharif Abuadbba, Zhi Zhang, Seyit Camtepe, Hyoungshick Kim, and Surya Nepal. Evaluation and optimization of distributed machine learning techniques for internet of things. *IEEE Transactions on Computers*, 2021.

Manuel Gil, Fady Alajaji, and Tamas Linder. Rényi divergence measures for commonly used univariate continuous distributions. *Information Sciences*, 249:124–131, 2013.

Antonious Girgis, Deepesh Data, and Suhas Diggavi. Renyi differential privacy of the subsampled shuffle model in distributed learning. *Advances in Neural Information Processing Systems*, 34, 2021.

Otkrist Gupta and Ramesh Raskar. Distributed learning of deep neural network over multiple agents. *Journal of Network and Computer Applications*, 116:1–8, 2018.

Kai Han, Yunhe Wang, Hanting Chen, Xinghao Chen, Jianyuan Guo, Zhenhua Liu, Yehui Tang, An Xiao, Chunjing Xu, Yixing Xu, et al. A survey on vision transformer. *IEEE Transactions on Pattern Analysis and Machine Intelligence*, 2022.

Ethan Harris, Antonia Marcu, Matthew Painter, Mahesan Niranjan, Adam Prügel-Bennett, and Jonathon S. Hare. Understanding and enhancing mixed sample data augmentation. *CoRR*, abs/2002.12047, 2020. URL `https://arxiv.org/abs/2002.12047`.

Zecheng He, Tianwei Zhang, and Ruby B Lee. Model inversion attacks against collaborative inference. In *Proceedings of the 35th Annual Computer Security Applications Conference*, pages 148–162, 2019.

Byeongho Heo, Sangdoo Yun, Dongyoon Han, Sanghyuk Chun, Junsuk Choe, and Seong Joon Oh. Rethinking spatial dimensions of vision transformers. *CoRR*, abs/2103.16302, 2021a. URL `https://arxiv.org/abs/2103.16302`.

Byeongho Heo, Sangdoo Yun, Dongyoon Han, Sanghyuk Chun, Junsuk Choe, and Seong Joon Oh. Rethinking spatial dimensions of vision transformers. In *Proceedings of the IEEE/CVF International Conference on Computer Vision*, pages 11936–11945, 2021b.

Zhenhou Hong, Jianzong Wang, Xiaoyang Qu, Jie Liu, Chendong Zhao, and Jing Xiao. Federated learning with dynamic transformer for text to speech. *arXiv preprint arXiv:2107.08795*, 2021.

Eunjeong Jeong, Seungeun Oh, Jihong Park, Hyesung Kim, Mehdi Bennis, and Seong-Lyun Kim. Hiding in the crowd: Federated data augmentation for on-device learning. *IEEE Intelligent Systems*, 36(5):80–87, 2020.

Peter Kairouz, H Brendan McMahan, Brendan Avent, Aurélien Bellet, Mehdi Bennis, Arjun Nitin Bhagoji, Kallista Bonawitz, Zachary Charles, Graham Cormode, Rachel Cummings, et al. Advances and open problems in federated learning. *Foundations and Trends® in Machine Learning*, 14(1–2):1–210, 2021.

Shigeki Karita, Nanxin Chen, Tomoki Hayashi, Takaaki Hori, Hirofumi Inaguma, Ziyan Jiang, Masao Someki, Nelson Enrique Yalta Soplin, Ryuichi Yamamoto, Xiaofei Wang, et al. A comparative study on transformer vs rnn in speech applications. In *2019 IEEE Automatic Speech Recognition and Understanding Workshop (ASRU)*, pages 449–456. IEEE, 2019.

Salman Khan, Muzammal Naseer, Munawar Hayat, Syed Waqas Zamir, Fahad Shahbaz Khan, and Mubarak Shah. Transformers in vision: A survey. *ACM Computing Surveys (CSUR)*, 2021.

Yusuke Koda, Jihong Park, Mehdi Bennis, Praneeth Vepakomma, and Ramesh Raskar. Airmixml: Over-the-air data mixup for inherently privacy-preserving edge machine learning. *arXiv preprint arXiv:2105.00395*, 2021.

Jakub Konečnỳ, Brendan McMahan, and Daniel Ramage. Federated optimization: Distributed optimization beyond the datacenter. *arXiv preprint arXiv:1511.03575*, 2015.

Jakub Konečnỳ, H Brendan McMahan, Felix X Yu, Peter Richtárik, Ananda Theertha Suresh, and Dave Bacon. Federated learning: Strategies for improving communication efficiency. *arXiv preprint arXiv:1610.05492*, 2016.

Alex Krizhevsky. Learning multiple layers of features from tiny images. Technical report, 2009.

Yann LeCun et al. Lenet-5, convolutional neural networks. *URL: http://yann. lecun. com/exdb/lenet*, 20(5):14, 2015.

Kangwook Lee, Hoon Kim, Kyungmin Lee, Changho Suh, and Kannan Ramchandran. Synthesizing differentially private datasets using random mixing. In *2019 IEEE International Symposium on Information Theory (ISIT)*, pages 542–546. IEEE, 2019.

Oscar Li, Jiankai Sun, Xin Yang, Weihao Gao, Hongyi Zhang, Junyuan Xie, Virginia Smith, and Chong Wang. Label leakage and protection in two-party split learning. *arXiv preprint arXiv:2102.08504*, 2021.

Tian Li, Anit Kumar Sahu, Ameet Talwalkar, and Virginia Smith. Federated learning: Challenges, methods, and future directions. *IEEE Signal Processing Magazine*, 37(3):50–60, 2020.

Ilya Loshchilov and Frank Hutter. Decoupled weight decay regularization. *arXiv preprint arXiv:1711.05101*, 2017.

Ilya Mironov. Rényi differential privacy. In *2017 IEEE 30th computer security foundations symposium (CSF)*, pages 263–275. IEEE, 2017.

Muhammad Muzammal Naseer, Kanchana Ranasinghe, Salman H Khan, Munawar Hayat, Fahad Shahbaz Khan, and Ming-Hsuan Yang. Intriguing properties of vision transformers. *Advances in Neural Information Processing Systems*, 34, 2021.

Milad Nasr, Reza Shokri, and Amir Houmansadr. Machine learning with membership privacy using adversarial regularization. In *Proceedings of the 2018 ACM SIGSAC conference on computer and communications security*, pages 634–646, 2018.

Seungeun Oh, Jihong Park, Sihun Baek, Hyelin Nam, Praneeth Vepakomma, Ramesh Raskar, Mehdi Bennis, and Seong-Lyun Kim. Differentially private cutmix for split learning with vision transformer. In *First Workshop on Interpolation Regularizers and Beyond at NeurIPS 2022*, 2022a. URL `https://openreview.net/forum?id=gRCWdltNQq`.

Seungeun Oh, Jihong Park, Praneeth Vepakomma, Sihun Baek, Ramesh Raskar, Mehdi Bennis, and Seong-Lyun Kim. Locfedmix-sl: Localize, federate, and mix for improved scalability, convergence, and latency in split learning. In *Proceedings of the ACM Web Conference 2022*, pages 3347–3357, 2022b.

Shraman Pal, Mansi Uniyal, Jihong Park, Praneeth Vepakomma, Ramesh Raskar, Mehdi Bennis, Moongu Jeon, and Jinho Choi. Server-side local gradient averaging and learning rate acceleration for scalable split learning. *arXiv preprint arXiv:2112.05929*, 2021.

Jihong Park, Sumudu Samarakoon, Anis Elgabli, Joongheon Kim, Mehdi Bennis, Seong-Lyun Kim, and Mérouane Debbah. Communication-efficient and distributed learning over wireless networks: Principles and applications. *Proceedings of the IEEE*, 109(5):796–819, 2021a.

Sangjoon Park, Gwanghyun Kim, Jeongsol Kim, Boah Kim, and Jong Chul Ye. Federated split task-agnostic vision transformer for covid-19 cxr diagnosis. *Advances in Neural Information Processing Systems*, 34, 2021b.

George-Liviu Pereteanu, Amir Alansary, and Jonathan Passerat-Palmbach. Split he: Fast secure inference combining split learning and homomorphic encryption. *arXiv preprint arXiv:2202.13351*, 2022.

Liangqiong Qu, Yuyin Zhou, Paul Pu Liang, Yingda Xia, Feifei Wang, Li Fei-Fei, Ehsan Adeli, and Daniel Rubin. Rethinking architecture design for tackling data heterogeneity in federated learning. *arXiv preprint arXiv:2106.06047*, 2021.

Alec Radford, Karthik Narasimhan, Tim Salimans, Ilya Sutskever, et al. Improving language understanding by generative pre-training. 2018.

Alec Radford, Jeffrey Wu, Rewon Child, David Luan, Dario Amodei, Ilya Sutskever, et al. Language models are unsupervised multitask learners. *OpenAI blog*, 1(8):9, 2019.

Md Atiqur Rahman, Tanzila Rahman, Robert Laganière, Noman Mohammed, and Yang Wang. Membership inference attack against differentially private deep learning model. *Trans. Data Priv.*, 11(1):61–79, 2018.

Ronald L Rivest, Len Adleman, Michael L Dertouzos, et al. On data banks and privacy homomorphisms. *Foundations of secure computation*, 4(11):169–180, 1978.

Reza Shokri, Marco Stronati, Congzheng Song, and Vitaly Shmatikov. Membership inference attacks against machine learning models. In *2017 IEEE symposium on security and privacy (SP)*, pages 3–18. IEEE, 2017.

Karen Simonyan and Andrew Zisserman. Very deep convolutional networks for large-scale image recognition. *arXiv preprint arXiv:1409.1556*, 2014.

Abhishek Singh, Praneeth Vepakomma, Otkrist Gupta, and Ramesh Raskar. Detailed comparison of communication efficiency of split learning and federated learning. *arXiv preprint arXiv:1909.09145*, 2019.

Nitish Srivastava, Geoffrey Hinton, Alex Krizhevsky, Ilya Sutskever, and Ruslan Salakhutdinov. Dropout: a simple way to prevent neural networks from overfitting. *The journal of machine learning research*, 15(1):1929–1958, 2014.

Andreas Steiner, Alexander Kolesnikov, Xiaohua Zhai, Ross Wightman, Jakob Uszkoreit, and Lucas Beyer. How to train your vit? data, augmentation, and regularization in vision transformers. *CoRR*, abs/2106.10270, 2021. URL `https://arxiv.org/abs/2106.10270`.

Chandra Thapa, Mahawaga Arachchige Pathum Chamikara, and Seyit Camtepe. Splitfed: When federated learning meets split learning. *CoRR*, abs/2004.12088, 2020a. URL `https://arxiv.org/abs/2004.12088`.

Chandra Thapa, Mahawaga Arachchige Pathum Chamikara, Seyit Camtepe, and Lichao Sun. Splitfed: When federated learning meets split learning. *arXiv preprint arXiv:2004.12088*, 2020b.

Hugo Touvron, Matthieu Cord, Matthijs Douze, Francisco Massa, Alexandre Sablayrolles, and Hervé Jégou. Training data-efficient image transformers & distillation through attention. *CoRR*, abs/2012.12877, 2020. URL `https://arxiv.org/abs/2012.12877`.

Ashish Vaswani, Noam Shazeer, Niki Parmar, Jakob Uszkoreit, Llion Jones, Aidan N Gomez, Łukasz Kaiser, and Illia Polosukhin. Attention is all you need. *Advances in neural information processing systems*, 30, 2017.

Praneeth Vepakomma, Otkrist Gupta, Tristan Swedish, and Ramesh Raskar. Split learning for health: Distributed deep learning without sharing raw patient data. *arXiv preprint arXiv:1812.00564*, 2018.

Vikas Verma, Alex Lamb, Christopher Beckham, Amir Najafi, Ioannis Mitliagkas, David Lopez-Paz, and Yoshua Bengio. Manifold mixup: Better representations by interpolating hidden states. In *International Conference on Machine Learning*, pages 6438–6447. PMLR, 2019.

Yu-Xiang Wang, Borja Balle, and Shiva Prasad Kasiviswanathan. Subsampled rényi differential privacy and analytical moments accountant. In *The 22nd International Conference on Artificial Intelligence and Statistics*, pages 1226–1235. PMLR, 2019.

Xiang Wu, Yongting Zhang, Minyu Shi, Pei Li, Ruirui Li, and Neal N Xiong. An adaptive federated learning scheme with differential privacy preserving. *Future Generation Computer Systems*, 127:362–372, 2022.

Han Xiao, Kashif Rasul, and Roland Vollgraf. Fashion-mnist: a novel image dataset for benchmarking machine learning algorithms. *arXiv preprint arXiv:1708.07747*, 2017.

Xin Yang, Jiankai Sun, Yuanshun Yao, Junyuan Xie, and Chong Wang. Differentially private label protection in split learning. *arXiv preprint arXiv:2203.02073*, 2022.

Sangdoo Yun, Dongyoon Han, Seong Joon Oh, Sanghyuk Chun, Junsuk Choe, and Youngjoon Yoo. Cutmix: Regularization strategy to train strong classifiers with localizable features. In *Proceedings of the IEEE/CVF International Conference on Computer Vision*, pages 6023–6032, 2019.

Hongyi Zhang, Moustapha Cisse, Yann N Dauphin, and David Lopez-Paz. mixup: Beyond empirical risk minimization. *arXiv preprint arXiv:1710.09412*, 2017.

Sixiao Zheng, Jiachen Lu, Hengshuang Zhao, Xiatian Zhu, Zekun Luo, Yabiao Wang, Yanwei Fu, Jianfeng Feng, Tao Xiang, Philip HS Torr, et al. Rethinking semantic segmentation from a sequence-to-sequence perspective with transformers. In *Proceedings of the IEEE/CVF conference on computer vision and pattern recognition*, pages 6881–6890, 2021.

Appendices

A List of Notations

Table 4: List of Notations.

Notation	**Meaning**
$\mathbb{C}$	a set of clients
n	# of clients
$\mathbb{D}_i$	dataset of the i-th client
$\mathbf{x}_i$	sample of the i-th client
$\mathbf{y}_i$	label of the i-th client
$\mathbf{w}_{c,i}$	lower model segment of the i-th client
$\mathbf{w}_s$	upper model segment of the server
P	patch size
N	# of patches
H, W, C	height, width, channels of image
$\mathbf{s}_i$	smashed data of the i-th client
D_s	dimension of $\mathbf{s}_i$
D_y	dimension of $\mathbf{y}_i$
$\mathbb{B}_i$	batch of the i-th client
b	batch size
η	learning rate
$\mathbf{M}_i$	binary on-off matrix for $\mathbf{s}_i$
k	mixing group size
$\mathbb{C}_k$	a set of mixing groups of size k
λ_i	mixing ratio of i-th client
α_M	mask distribution
α_D	dataset distribution
$\tilde{\mathbf{s}}_{\{i,i'\}}$	i-th DP-CutMix smashed data
$\bar{\mathbf{s}}'_i$	i-th DP-Cutout smashed data
$n_{s,i}$	the i-th zero-mean Gaussian matrix with variance σ_s^2 and size D_s
$n_{y,i}$	the i-th zero-mean Gaussian matrix with variance σ_y^2 and size D_y
α	RDP parameter
δ	DP parameter
Δ	pixel-wise upper bound

B Visualization of Additional Images

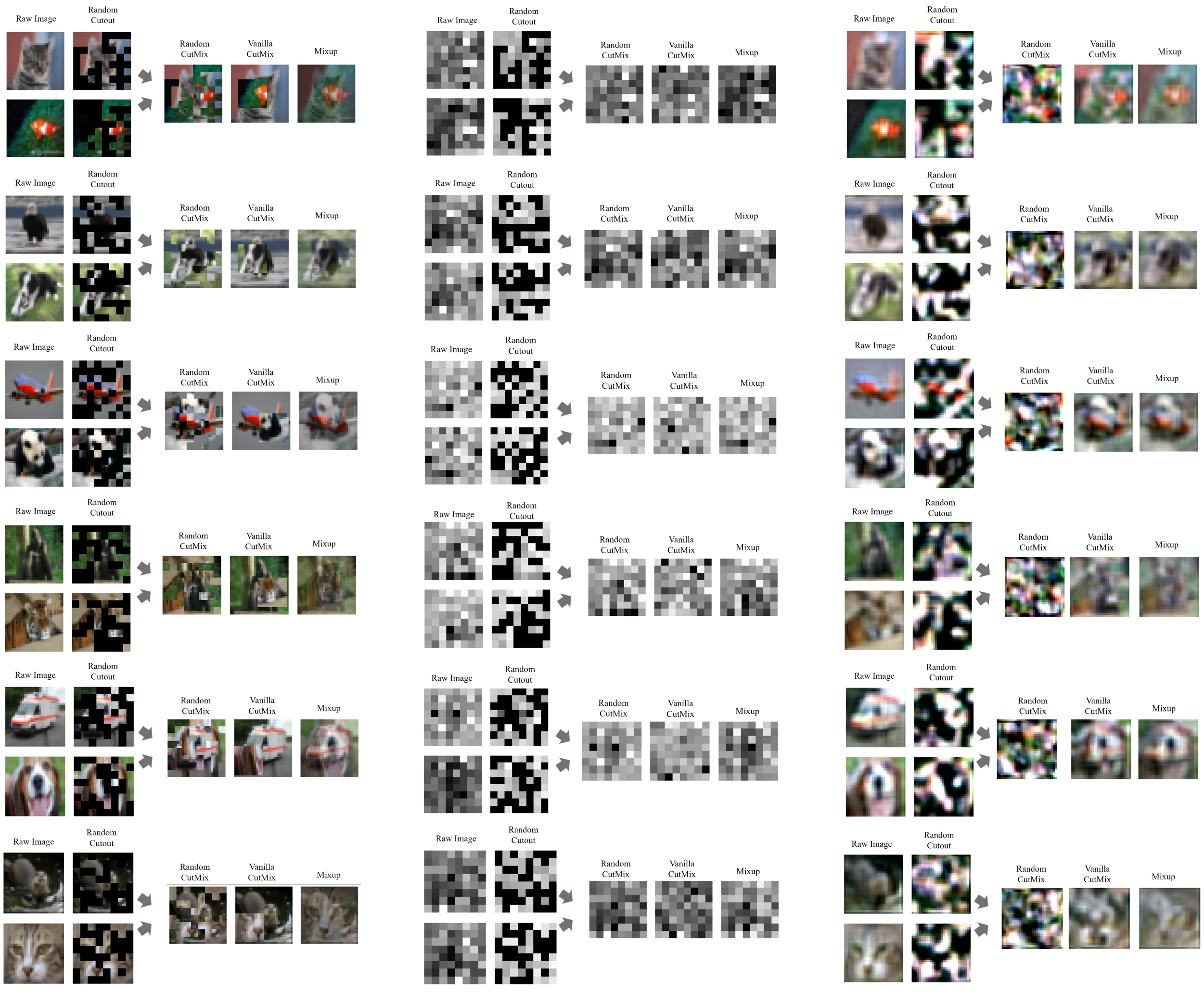

(a) Raw data.

(b) Smashed data.

(c) Restored data.

Figure 12: Additional example images for various regularization techniques.

C Accuracy comparison of regularizations applied to the input layer

Table 5: Top-1 accuracy of SL-based methods for various datasets and models.

Method	Models w/ CIFAR-10			Models w/ Fashion-MNIST		
	ViT-Tiny	PiT-Tiny	VGG-16	ViT-Tiny	PiT-Tiny	VGG-16
PSL w. Mixup	74.36	37.21	66.08	89.86	87.62	89.70
PSL w. Random Cutout	22.03	45.19	66.32	88.65	88.51	89.62
PSL w. Vanilla CutMix	73.02	33.54	47.69	88.72	88.37	90.02
CutMixSL (proposed)	**75.06**	**53.93**	**67.43**	**89.91**	**89.53**	**90.32**